
Supervised Quadratic Feature Analysis: Information Geometry for Dimensionality Reduction

Daniel Herrera-Esposito
Department of Psychology
University of Pennsylvania
Philadelphia, PA 19104
dherresp@sas.upenn.edu

Johannes Burge
Department of Psychology
University of Pennsylvania
Philadelphia, PA 19104
jburge@psych.upenn.edu

Abstract

Supervised dimensionality reduction aims to map labeled data to a low-dimensional feature space while maximizing class discriminability. Directly computing discriminability is often impractical, so an alternative approach is to learn features that maximize a distance or dissimilarity measure between classes. The Fisher-Rao distance is an important information geometry distance in statistical manifolds. It is induced by the Fisher information metric, a tool widely used for understanding neural representations. Despite its theoretical and practical appeal, Fisher-Rao distances between classes have not been used as a maximization objective in supervised feature learning. Here, we present Supervised Quadratic Feature Analysis (SQFA), a linear dimensionality reduction method that maximizes Fisher-Rao distances between class distributions, by exploiting the information geometry of the symmetric positive definite manifold. SQFA maximizes distances using first- and second-order statistics, and its features allow for quadratic discriminability (i.e. QDA performance) matching or surpassing state-of-the-art methods on real-world datasets. We theoretically motivate Fisher-Rao distances as a proxy for quadratic discriminability, and compare its performance to other popular distances (e.g. Wasserstein distances). SQFA provides a flexible state-of-the-art method for dimensionality reduction. Its successful use of Fisher-Rao distances between classes motivates future research directions.

1 Introduction

Consider a labeled random variable $\mathbf{x} \in \mathbb{R}^n$ with label $y \in \{1, \dots, c\}$, where c is the number of classes. Supervised dimensionality reduction aims to map the high-dimensional variable \mathbf{x} to a lower dimensional variable $\mathbf{z} \in \mathbb{R}^m$ that best supports classification performance, or discriminability. Despite the availability of methods for learning non-linear features, like deep neural networks [32] and manifold learning [50], these methods require large volumes of data and their features are often difficult to interpret. Methods that learn linear features are better understood theoretically, and often support good performance, making them a popular choice for many applications [16].

Directly maximizing discriminability in the reduced-dimensional feature space is often impractical [23]. An alternative approach is to maximize, as a proxy for discriminability, a distance or dissimilarity measure between the probability distributions associated with each class in this space. For example, Linear Discriminant Analysis (LDA) learns linear features that maximize the pairwise squared Euclidean distances between the class means, after whitening the average within-class covariance. Other methods take a similar approach, but use different distances or dissimilarity measures that can learn features that support better classification performance than LDA [11, 19, 48, 22].

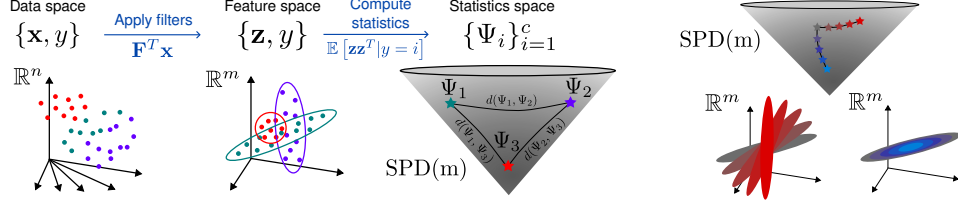


Figure 1: SQFA learns features using an information geometry objective. **Left.** SQFA and smSQFA map the n -dimensional data into an m -dimensional feature space using the linear filters \mathbf{F} . In smSQFA, the class-specific second-moment matrices of the features are represented as points in the $\text{SPD}(m)$ manifold (which is an open cone). Fisher-Rao distances in $\text{SPD}(m)$ are used for learning. **Right.** Each point in $\text{SPD}(m)$ (top) corresponds to a second-moment ellipse (below). As the distance in $\text{SPD}(m)$ increases, the second-order statistics become more different and more discriminable.

Information geometry considers probability distributions as points in a statistical manifold, providing a natural framework for measuring distances between them [41]. To determine distances in the manifold, a Riemannian metric is required. The Fisher information metric, a principled measure of local discriminability, can be used for measuring distances. This metric has recently proven useful to study the geometry of representations in both machine learning [33, 56, 4] and neuroscience [44, 31, 18, 21, 54, 53, 60, 61], and it induces the Fisher-Rao distance, a particularly important and well-studied distance in manifolds of probability distributions [46, 1, 41]. Given the growing interest in the geometry of neural representations [31, 44, 59, 12] and the significance of the Fisher-Rao metric to this geometry, Fisher-Rao distance maximization is a natural objective for dimensionality reduction in machine learning and neuroscience.

Despite its theoretical and practical appeal, maximization of Fisher-Rao distances between classes has not been used for dimensionality reduction. One possible reason is that, although the Fisher information metric can be interpreted in terms of local (threshold-level) discriminability via the Cramer-Rao bound [17], the Fisher-Rao distance does not have a formal interpretation familiar to neuroscience and machine learning [15]. Another possible reason is the lack of closed-form expressions for the Fisher-Rao distance between multivariate Gaussians with arbitrary means and covariances [36, 42]; however, an exact expression exists for the special case of zero-mean Gaussians (see below) [5].

Here, we present Supervised Quadratic Feature Analysis (SQFA), a supervised dimensionality reduction method that learns linear features that support quadratic discriminability (i.e. QDA performance) by maximizing Fisher-Rao distances between class-conditional distributions under Gaussian assumptions. For this, SQFA uses a closed-form approximation to the Fisher-Rao distance between arbitrary Gaussians [8, 42], and an exact expression for the special case of zero-mean Gaussians [5], both which make use of the information geometry of the symmetric positive definite (SPD) manifold [52]. SQFA features allow for high quadratic discriminability of classes in three real-world datasets, better than, or comparable to, features learned with other distances and state-of-the-art methods. These results show that the Fisher-Rao distance is a good proxy for discriminability, providing a novel use case as well as a useful interpretation of this distance for future work in the field.

2 Model

Notation. The class-conditional means and covariances of the variable \mathbf{x} are denoted by $\gamma_i = \mathbb{E}[\mathbf{x}|y=i]$ and $\Phi_i = \mathbb{E}[(\mathbf{x} - \gamma_i)(\mathbf{x} - \gamma_i)^T|y=i]$, respectively. The low-dimensional projection of \mathbf{x} is given by $\mathbf{z} = \mathbf{F}^T \mathbf{x}$, where $\mathbf{F} \in \mathbb{R}^{n \times m}$ is a matrix of filters, and the respective class-conditional means, second moments, and covariances are given by $\mu_i = \mathbb{E}[\mathbf{z}|y=i]$, $\Psi_i = \mathbb{E}[\mathbf{z}\mathbf{z}^T|y=i]$, and $\Sigma_i = \Psi_i - \mu_i \mu_i^T$. We also denote by θ_i the parameters $p(\mathbf{z}|y=i)$, or equivalently $p(\mathbf{z}|\theta_i)$, in some cases representing the mean and covariance of a Gaussian distribution.

2.1 Information geometry approach for second moments

Our goal is to find linear filters \mathbf{F} such that the class-conditional first- and second-order statistics of the low-dimensional variable $\mathbf{z} = \mathbf{F}^T \mathbf{x}$ maximize quadratic discriminability (i.e. ability to correctly categorize samples using a quadratic classifier). To achieve this, we use the information geometric approach of maximizing pairwise distances between the class-conditional distributions in the feature space. For ease of explanation, we first illustrate the approach with a simple model—second-moments SQFA (smSQFA)—that uses only the class-conditional second-moment matrices Ψ_i , and which is appropriate for the zero-mean Gaussian case. Later, we present the full model—SQFA— that uses both the class means and covariances (μ_i and Σ_i).

Second-moment matrices Ψ_i define points in the manifold of m -by- m SPD matrices, denoted $\text{SPD}(m)$ (Figure 1) [52]. This manifold can also be interpreted as the manifold of zero-mean Gaussian distributions $\mathcal{N}(\mathbf{0}, \Psi_i)$ because, in the zero-mean case, the second moment matrices equal the covariance matrices $\Sigma_i = \Psi_i$ and completely parametrize these distributions. $\text{SPD}(m)$ can be used to measure Riemannian distances $d(\Psi_i, \Psi_j)$ between the classes. The intuition behind our approach is that a larger distance $d(\Psi_i, \Psi_j)$ indicates that the classes are more different, and suggests that they should be more discriminable (Figure 1). The sum of pairwise distances relates to the overall discriminability, and can be used as an objective function

$$\arg \max_{\mathbf{F} \in \mathbb{R}^{n \times m}} \sum_{i=1}^c \sum_{j=1}^c d(\Psi_i, \Psi_j) \quad (1)$$

Many distances are compatible with $\text{SPD}(m)$, but it is important for $d(\Psi_i, \Psi_j)$ to be a good proxy for discriminability. Below, we show that the Fisher-Rao distance is just such a proxy.

2.2 Fisher-Rao distance as accumulated local discriminability

For distribution $p(\mathbf{z}|\theta)$, the Fisher information in the direction θ' is defined as $\mathcal{I}_\theta(\theta') = \mathbb{E}[(s(\mathbf{z}, \theta) \cdot \theta')^2]$, where the expectation is taken over \mathbf{z} , and $s(\mathbf{z}, \theta) = \nabla_\theta \log p(\mathbf{z}|\theta)$ is the score function. The quantity $\sqrt{\mathcal{I}_\theta(\theta')}$ is a measure of how discriminable $p(\mathbf{z}|\theta)$ is from $p(\mathbf{z}|\theta + \epsilon\theta')$, where $\epsilon\theta'$ is an infinitesimal perturbation, and it is commonly used in signal processing and in neuroscience to measure the local discriminability of a signal or stimulus θ given an observation or neural response \mathbf{z} [17, 37, 57, 53, 40].

Let the curve $\Psi(t) \in \text{SPD}(m)$ be the Fisher-Rao geodesic (i.e. the shortest curve) from $\mathcal{N}(\mathbf{0}, \Psi_i)$ to $\mathcal{N}(\mathbf{0}, \Psi_j)$, where $\Psi(0) = \Psi_i$, $\Psi(1) = \Psi_j$, and $\Psi'(t)$ is the velocity vector at point $\Psi(t)$. The Fisher-Rao distance between Ψ_i and Ψ_j , denoted $d_{FR}(\Psi_i, \Psi_j)$, is obtained by integrating the speed along the geodesic, $d_{FR}(\Psi_i, \Psi_j) = \int_0^1 \|\Psi'(t)\| dt$. The Fisher information metric defines the norm of a velocity vector as $\|\theta'\| = \sqrt{\mathcal{I}_\theta(\theta')}$, which in the zero-mean Gaussian case is given by

$$\|\Psi'(t)\| = \sqrt{\mathcal{I}_{\Psi(t)}(\Psi'(t))} = \sqrt{0.5 \text{Tr}(\Psi(t)^{-1} \Psi'(t) \Psi(t)^{-1} \Psi'(t))} \quad (2)$$

Then, $\|\Psi'(t)\|$ is a measure of the discriminability between $\mathcal{N}(\mathbf{0}, \Psi(t))$ and $\mathcal{N}(\mathbf{0}, \Psi(t + dt))$, and the Fisher-Rao distance can be expressed as $d_{FR}(\Psi_i, \Psi_j) = \int_0^1 \sqrt{\mathcal{I}_{\Psi(t)}(\Psi'(t))} dt$, which can be conceptualized as the accumulated discriminability of the infinitesimal perturbations transforming $\mathcal{N}(\mathbf{0}, \Psi_i)$ into $\mathcal{N}(\mathbf{0}, \Psi_j)$ along the geodesic, making it a sensible proxy for discriminability.

The Fisher-Rao distance between zero-mean Gaussians coincides (up to a factor of $\sqrt{2}$) with the affine-invariant distance in $\text{SPD}(m)$ [5], given by

$$d_{AI}(\Psi_i, \Psi_j) = \left\| \log(\Psi_i^{-1/2} \Psi_j \Psi_i^{-1/2}) \right\|_F = \sqrt{\sum_{k=1}^m \log^2 \lambda_k} = \sqrt{2} d_{FR}(\Psi_i, \Psi_j) \quad (3)$$

where \log is the matrix logarithm, $\|\cdot\|_F$ is the Frobenius norm, and λ_k is the k -th generalized eigenvalue of the pair of matrices (Ψ_i, Ψ_j) (see Appendix A.1 for further discussion of the generalized eigenvalues and discriminability). In supplementary analyses, we compare $d_{FR}(\Psi_i, \Psi_j)$ to other $\text{SPD}(m)$ distances and dissimilarity measures previously used for dimensionality reduction [11, 20] (Appendix A.2), and directly compare it to the Bayes error for the 1D and 2D cases (Appendix A.3), supporting its usefulness as a proxy for discriminability. smSQFA uses $d_{AI}(\Psi_i, \Psi_j)$ in the objective function of Equation 1.

2.3 Fisher-Rao distances for arbitrary Gaussian distributions

The reasoning developed in the previous section applies to the case of Gaussians with arbitrary means, which are parametrized by $\theta_i = (\mu_i, \Sigma_i)$. Such Gaussians can be considered as points in the product manifold $\mathbb{R}^m \times \text{SPD}(m)$. Unfortunately, there is no closed-form expression for the Fisher-Rao distance $d_{FR}(\theta_i, \theta_j)$ in this general case [42]. However, Calvo and Oller [8] derived a lower bound for the distance between m -dimensional Gaussians by embedding θ into $\text{SPD}(m+1)$ as

$$\Omega = \begin{bmatrix} \Sigma + \mu\mu^T & \mu \\ \mu^T & 1 \end{bmatrix} \quad (4)$$

where $d_{FR}(\theta_i, \theta_j) \geq d_{AI}(\Omega_i, \Omega_j)$. This bound is a good approximation to $d_{FR}(\theta_i, \theta_j)$ [42]. More accurate approximations are available via numerical methods, but these require more elaborate and computationally costly implementations [42, 43]. SQFA uses the Calvo-Oller bound in Equation 1. Notably, the Calvo-Oller bound can be easily extended to some other distributions (e.g. multivariate t-Student and Cauchy distributions) [9, 42].

2.4 Homoscedastic Gaussians: LDA is a special case of SQFA

In the special case of Gaussians with arbitrary means and fixed covariance $\Sigma = \Sigma_i = \Sigma_j$ ¹, the Fisher-Rao distance between $\mathcal{N}(\mu_i, \Sigma)$ and $\mathcal{N}(\mu_j, \Sigma)$ is the Mahalanobis distance $d_{\Sigma}(\mu_i, \mu_j) = \sqrt{(\mu_i - \mu_j)^T \Sigma^{-1} (\mu_i - \mu_j)}$ [46]. LDA can be interpreted as maximizing the pairwise squared Euclidean distances between the means after whitening (see Introduction). LDA can be equivalently described as maximizing the pairwise squared Mahalanobis distances in this special case. LDA is thus a special case of SQFA (see Appendix B for a proof)². This information geometric view of LDA further supports the use of Fisher-Rao distances for dimensionality reduction.

2.5 Learning

Optimization. Filters \mathbf{F} were optimized by maximizing Equation 1 with the L-BFGS algorithm until the change in the loss was less than 10^{-6} for three consecutive iterations. Filters were constrained to have unit norm, and were initialized to the m first PCA components. This optimization problem is non-convex, so the solution may depend on the initialization. To compute the class-conditional statistics in the low-dimensional feature space, the filters are applied to the means and covariances of the high-dimensional raw data (i.e. γ_i and Φ_i). Namely, $\mu_i = \mathbf{F}^T \gamma_i$ and $\Sigma_i = \mathbf{F}^T \Phi_i \mathbf{F}$. For the current datasets, optimization was performed on a consumer laptop in seconds.

Data preprocessing. For the digit recognition datasets, the mean of the training set was subtracted from the data, and then the pixels were normalized by average standard deviation. For the speed estimation dataset, the preprocessing of the original work [7] was used (Appendix F).

Regularization and invariance. To prevent rank-deficient or ill-conditioned covariances (and second-moment matrices), a regularization term was used such that $\Sigma_i = \mathbf{F}^T \Phi_i \mathbf{F} + \mathbf{I}_m \sigma^2$, where \mathbf{I}_m is the identity matrix, and σ^2 is the regularization parameter. Regularization makes training more stable and improves performance in our experiments, but it can mask relevant information in low-variance subspaces. The hyperparameter σ^2 was set manually for each dataset to maximize performance, except for the speed estimation dataset, where it was chosen to match the biologically-informed value used in the original work [7]. The parameter values for the SVHN, MNIST, and speed datasets were 0.01, 0.01, and 0.001, respectively. Future work should explore methods for automatic regularization. See Appendix A.2.3 for results on robustness to the choice of σ^2 . Future work should explore automatic regularization methods.

Fisher-Rao distances are invariant to invertible linear transformations of the feature vector. This implies that the solution to Equation 1 is only unique up to the subspace spanned by the filters. When regularization is used, however, the invariance no longer holds. See Appendix C for proofs and a discussion of the benefits and drawbacks of invariance and regularization.

¹This 'special case' refers to the distance along the sub-manifold of Gaussians with fixed covariance Σ . The distance along the full Gaussian manifold is a non-linear function of the Mahalanobis distance[46].

²SQFA uses Fisher-Rao distances, which we found to perform better than squared distances. Thus, LDA is actually a special case of a variant of SQFA that uses squared Fisher-Rao distances.

The ordering of the filters is not unique. In some applications, it is desirable for filters to be rank-ordered by usefulness. Such ordering can, for example, be achieved by learning the filters in pairs. If two filters are learned first, then this pair can be fixed and two more can be learned, and so on. This procedure will return pairs that are ordered by how well they support class discriminability.

Comparison to other methods. We compared SQFA to other dimensionality reduction methods. Each method learned a set of filters and performance accuracy was computed with the QDA classifier. We compared SQFA to the following commonly used methods: PCA, LDA, Independent Component Analysis (ICA) and Factor Analysis (FA). We also compared to a state-of-the-art method for finding features that maximize QDA accuracy [11], which we call Bhattacharyya distance maximization (BDM)³, and to a state-of-the-art method for learning linear features that maximize the performance of kNN classifiers called Large Margin Nearest Neighbors (LMNN) [58]⁴.

We used scikit-learn implementations of PCA, LDA, ICA, FA, and the QDA classifier [45], and the metric-learn library for LMNN [55]. For LDA, we set the shrinkage regularization parameter manually to maximize QDA accuracy. For BDM filter learning, we substituted the Bhattacharyya distance for the Fisher-Rao distance and otherwise used our implementation of SQFA.

A Python package implementing SQFA can be found at <https://github.com/dherrera1911/sqfa>.

3 Related work

The approach of maximizing a distance or dissimilarity measure between classes in a low-dimensional feature space is common in supervised dimensionality reduction. The canonical supervised dimensionality reduction method, LDA, maximizes the pairwise Mahalanobis distances between the class means, under the assumption that the within-class covariances are identical (Section 2.4, Appendix B), to maximize linear discriminability. Other methods use distances or dissimilarity metrics that allow for different class-conditional covariances to learn features that aim to maximize quadratic discriminability [20]. Of these, maximization of the Bhattacharyya distance [11] and the Chernoff distance [19, 48, 51] are successful approaches. The Chernoff distance between two Gaussian distributions $\mathcal{N}(\boldsymbol{\mu}_i, \boldsymbol{\Sigma}_i)$ and $\mathcal{N}(\boldsymbol{\mu}_j, \boldsymbol{\Sigma}_j)$ is given by

$$d_C(s) = \frac{s(1-s)}{2}(\boldsymbol{\mu}_i - \boldsymbol{\mu}_j)^T \boldsymbol{\Sigma}(s)^{-1}(\boldsymbol{\mu}_i - \boldsymbol{\mu}_j) + \frac{1}{2} \log \frac{\det(\boldsymbol{\Sigma}(s))}{\det(\boldsymbol{\Sigma}_i)^s \det(\boldsymbol{\Sigma}_j)^{1-s}} \quad (5)$$

where $\boldsymbol{\Sigma}(s) = s\boldsymbol{\Sigma}_1 + (1-s)\boldsymbol{\Sigma}_2$. The formula $\exp^{-d_C(s)}$ gives an upper bound on the Bayes error of a classifier for the two distributions [23], and $s \in [0, 1]$ can be optimized to minimize the bound (although s is often set to predetermined values [19, 48]). The Bhattacharyya distance is obtained by setting $s = 0.5$. Because larger Chernoff and Bhattacharyya distances imply smaller upper bounds on the Bayes error, they are sensible measures of discriminability [23].

Other methods learn features that optimize for more complex criteria of class separation, like the performance of kNN classifiers. One example is Wasserstein Discriminant Analysis (WDA), which maximizes the regularized Wasserstein distance between the class-conditional empirical distributions [22]. One difference between the Wasserstein and the Fisher-Rao distance is that the former is dependent on the choice and scale of the data axes, because it is not invertible to linear transformations. In supplementary analyses we show that the Wasserstein distance leads to poor quadratic discriminability in the datasets tested here (see Appendix A.2).

Although WDA and other existing techniques like metric learning methods [58] can learn linear features with more complex class separability than SQFA, the latter has important advantages. First, SQFA operates only on the class-conditional first- and second-order data statistics, and not on the raw data itself. Second, the computational cost of SQFA is lower, and its cost does not scale with the number of data points per class. This can be a substantial benefit for some applications (see Discussion). Third, quadratic classifiers based on Gaussian assumptions (i.e. QDA) are often more interpretable than kNN classifiers.

³If all the class priors are equal, BDM is also equivalent to the Duin and Loog [19] method maximizing Chernoff distances.

⁴To train LMNN we used the first 100 principal components of the data and 10% of the samples, because the high computational cost. Results for the other methods were similar when using the same reduced dataset.

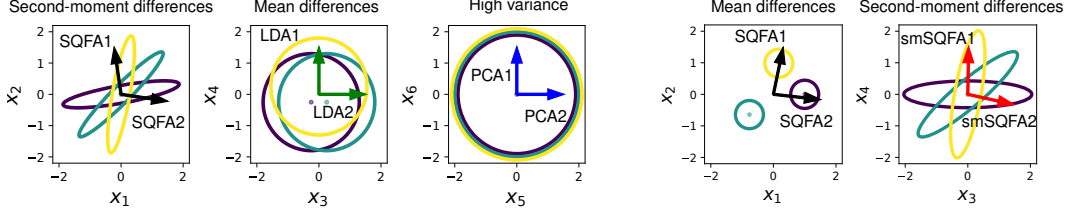


Figure 2: Ellipses represent Gaussian-distributed raw data for three classes (colors). Each panel shows two data-dimensions, where the classes are distinguished by different statistical properties. Arrows represent the filters learned by different methods. **Left.** Toy problem 1. 6D data, where the classes are distinguished by large covariance differences (dimensions 1-2), small mean differences (dimensions 3-4), or neither (dimensions 5-6). We learned two filters each with SQFA, LDA, and PCA. Only SQFA prefers the most discriminative subspace (dimensions 1-2). **Right.** Toy problem 2. 4D data, where the second-moment matrices are slightly more different in dimensions 3-4, but the large mean differences make dimensions 1-2 more discriminative. We learned two filters with SQFA and smSQFA. The SQFA filters select for the most discriminative subspace (dimensions 1-2).

Geometry-aware PCA (gaPCA) also deserves special mention because of its algorithmic similarity with SQFA. gaPCA is an unsupervised dimensionality reduction method for data in $\text{SPD}(m)$ [24]. For a dataset $\{\mathbf{X}_q\}_{q=1}^N$ where each observation $\mathbf{X}_q \in \text{SPD}(n)$, gaPCA maps the data to a lower dimensional manifold $\text{SPD}(m)$ using $\mathbf{Z}_q = \mathbf{F}^T \mathbf{X}_q \mathbf{F}$. The set of learned filters \mathbf{F} maximize the variance of the transformed dataset $\{\mathbf{Z}_q\}_{q=1}^N$. Although the goals of gaPCA and SQFA are very different, the optimization problem is almost identical in the case where pairwise squared affine-invariant distances are used to compute the variance in gaPCA analogous to Equation 1 [14]. SQFA might benefit from some of the tools developed for gaPCA [14].

4 Results

4.1 Toy problem: SQFA vs. LDA vs. PCA

First, we illustrate the differences between SQFA, LDA, and PCA with toy datasets. The first dataset has three classes and six dimensions. It is designed such that each of three different two-dimensional subspaces are preferred by one of the three techniques (Figure 2). Dimensions 1-2 contain very different and discriminable within-class covariances, so these dimensions are favored by SQFA. In these dimensions, however, there are no differences in the within-class means and the generalized variance across classes is low, so they are non-preferred by LDA and PCA. Dimensions 3-4 contain differences in the within-class means, so they are preferred by LDA. But these dimensions do not support good discrimination and have only moderate generalized variance, so they are non-preferred by SQFA and PCA. Dimensions 5-6 contain high variance, so they are preferred by PCA, but they do not support discrimination at all. Each method learns filters that select for the expected subspace. The SQFA filters select for the most discriminative subspace.

Next, with a second toy dataset having four dimensions, we compare SQFA and smSQFA. Dimensions 1-2 and dimensions 3-4 have second-moment matrices that are nearly same, but very different means and covariances. In dimensions 1-2, the classes have different means and the same covariance. In dimensions 3-4, the classes have different covariances and the same mean. SQFA learns its first two filters in the first two dimensions because they support the best discrimination, due to the widely separated means and low covariance (Figure 2). smSQFA learns filters in dimensions 3-4 because the second-moment matrices in those dimensions are slightly more different than in dimensions 1-2, and because smSQFA is blind to mean differences. Hence, SQFA flexibly selects features that are most useful for class discrimination, regardless of where the information lies.

4.2 SQFA for digit classification with poor first-order information

To examine how SQFA performs on a real-world dataset, we compared SQFA to other methods using the Street View House Numbers (SVHN) dataset. For each of eight methods, we learned nine

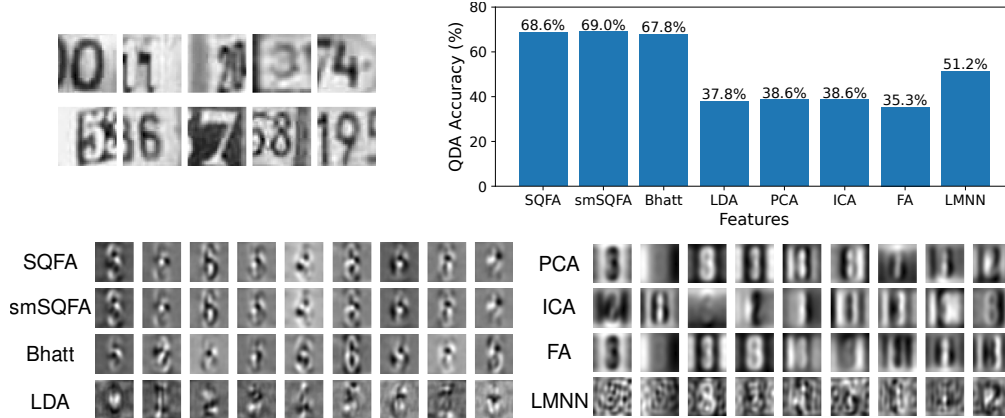


Figure 3: SQFA extracts useful features using class-conditional second-order statistics, outperforming related methods. **Top left.** Example images from SVHN. **Top right.** QDA accuracy using the features learned by the different methods. **Bottom.** Filters learned with different methods.

filters and quantified digit classification performance with a QDA classifier (Figure 3). (LDA can learn only $c - 1$ filters where c is the number of classes; hence, nine filters were learned.) SQFA and smSQFA features support the highest classification performance, outperforming even the features learned by BDM, a state-of-the-art method for maximizing quadratic discriminability⁵ [11, 19]. SQFA and smSQFA were also among the fastest to learn the features (Appendix D). The many sources of variation in the images (e.g. digits with mixed contrast polarity, variation in background intensity), entailed that first-order differences provided poor signals for discriminating between the digits. Second-order differences support much better discrimination performance.

4.3 SQFA for digit classification with useful first-order information

To examine how SQFA classifies digits when both first- and second-order statistics are informative, we compared the same eight methods using the MNIST dataset (Figure 4). SQFA, BDM, and LMNN, yielded the best performance with near-identical accuracies across the three methods⁶. SQFA outperforms both smSQFA and LDA. smSQFA uses the within-class second-moments but not the means; LDA uses the within-class means but not the second moments. Why do the MNIST and SVHM datasets have different statistical properties? In MNIST, there are many fewer within-class sources of variability—the digits are always white on black backgrounds. In these circumstances, the different amount of ‘ink’ required to scrawl each digit makes it highly likely that the mean pixel value (or other first-order feature) provides useful information for the task. The pattern of results indicates that first- and second-order information indeed both carry useful information for the task, and that SQFA exploits these two information sources to learn discriminative features.

4.4 Naturalistic speed estimation task

Next, we examine how SQFA features compare to optimal features for quadratic discrimination. To answer this question, we tested SQFA with a dataset used to investigate the neural computations underlying speed estimation [7, 10, 26]. This video-based dataset is interesting for several reasons. First, finding features (receptive fields) that are useful for solving visual tasks is essential for systems neuroscience and perception science [6], which is a potential application area for SQFA. Second, the within-class means approximately equal zero and the task-relevant information is in the covariance structure. SQFA can thus use an exact expression for—rather than a bound on—the Fisher-Rao distance during feature learning (see Sections 2.2 & 2.3). Third, SQFA filters and decoding performance can be directly compared to results obtained with a method called AMA-Gauss [28]. AMA-Gauss learns features that maximize the performance of a Bayesian decoder that directly optimizes quadratic

⁵SQFA and smSQFA also outperform BDM on simulated within-class Gaussian data (Appendix E)

⁶Feature learning via LMNN was considerably slower than the other best-performing methods (Appendix D).

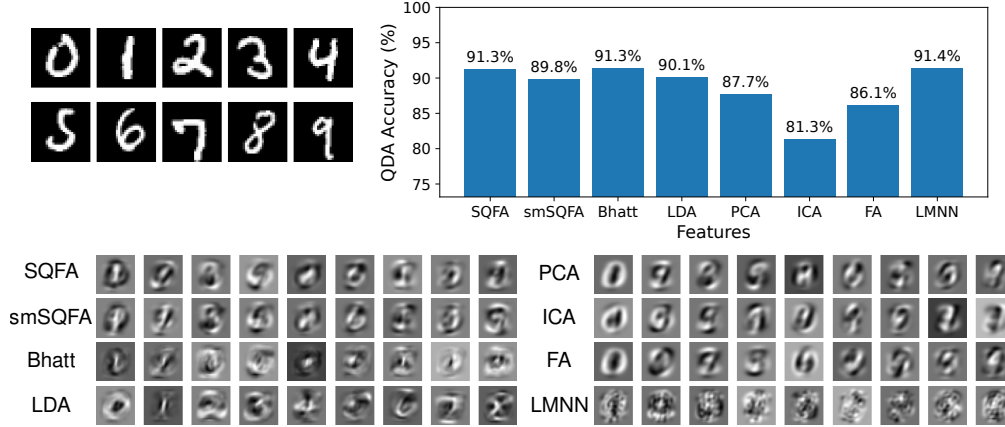


Figure 4: SQFA can exploit class-conditional first- and second-order information. **Top left.** Example images from MNIST. **Top right.** QDA accuracy using the features learned by the different methods. **Bottom.** Filters learned with different methods.

decoding performance, rather than a proxy for it (i.e. Fisher-Rao distance). AMA-Gauss filters and performance thus provide a principled benchmark for comparison (see Appendix F for more details on the dataset and AMA-Gauss).

Each video in the dataset consists of 30 horizontal pixels and 15 frames. The vertical dimension was averaged out. Hence, the videos can be represented as 2D space-time plots (Figure 5). Each video shows a naturally textured surface moving with one of 41 different speeds (i.e. classes). SQFA filters were learned in sequential pairs to aid interpretability (see Section 2.5).

SQFA, smSQFA, AMA-Gauss, and BDM learn filters that are similar to typical motion-sensitive receptive fields in visual cortex, selecting for a range of spatio-temporal frequencies [38, 49, 47]. The filters learned by the other methods, in contrast, either lack clear motion sensitivity, or do not cover a range of spatio-temporal frequencies (Figure 5).

SQFA and smSQFA features support better performance than those learned by all other methods, except for AMA-Gauss. There are two issues that very likely underlie this performance gap. First, despite the fact that Fisher-Rao distance is a good proxy for the discriminability of two classes, it is not perfect (Appendix A.3). Second, summing the pairwise discriminabilities (i.e. distances) often does not accurately reflect discriminability in multi-class problems [34, 51]. AMA-Gauss, on the other hand, is not hampered by either of these issues because it directly optimizes multi-class classification accuracy.

5 Discussion

We have introduced SQFA, a supervised dimensionality reduction method for learning linear features that support quadratic classifiers, like QDA. With three different real-world datasets, we showed that SQFA can learn features that support quadratic classification accuracy that is better than, or on par with, the performance obtained with other well-established methods, with a computational cost comparable to standard linear dimensionality reduction methods. SQFA is based on a novel information geometric approach that maximizes the Fisher-Rao distances between class-conditional statistics under Gaussian assumptions.

A useful property of SQFA is that it requires only the first- and second-order class-specific statistics of the data, rather than samples of the data. Thus, it can be used when class-conditional statistics are available but the raw data itself is not (e.g. unlike AMA-Gauss or LMNN that operate on the raw data). A possible application of this is in neuroscience, where recent modeling work allows the estimation of the covariance structure of neural responses in unobserved experimental conditions [39, 18, 35], and where second-order response statistics are known to be essential to neural coding [37, 30]. In this context, SQFA can be used for the identification of the modes of neural population

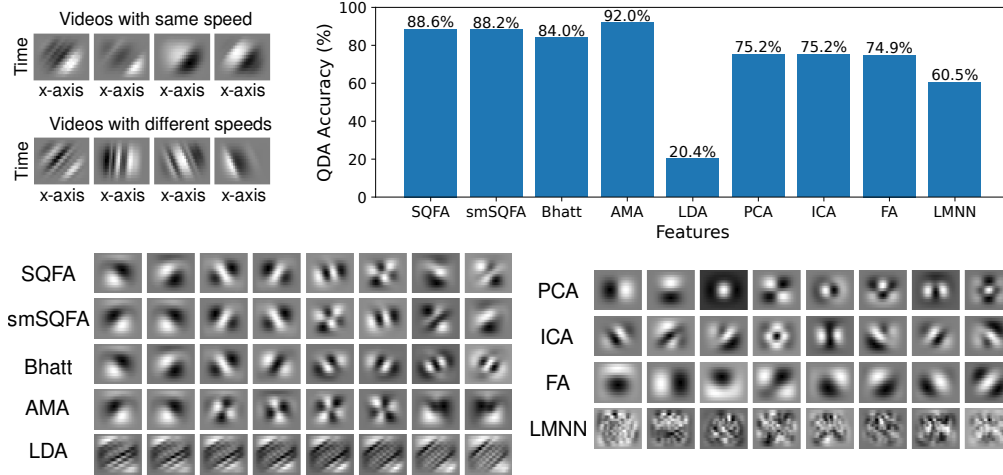


Figure 5: SQFA features are close to optimal for quadratic discrimination. **Top left.** 4 example videos with the same speed (left) and 4 example videos with different speeds (right). Each video is shown as a 2D space-time plot where the vertical axis is time and the horizontal axis is space. **Top right.** Performance of a QDA classifier using the filters learned by the different methods. **Bottom.** Filters learned different methods (each image shows a 2D space-time plot).

activity that are most useful for decoding by downstream neural circuits, a problem that is of interest in systems neuroscience.

A particularly appealing feature of the Fisher-Rao distance is that it is the Riemannian distance induced by the Fisher information metric [1, 41]. This metric is a well-established tool for studying neural representations [17], their local geometry [31, 56, 4, 18, 21], and how they relate to perception [57, 61, 53]. Given the widespread use of the Fisher information metric for local geometric analyses, and given that the Fisher-Rao distance is the Riemannian distance that is induced by this metric, the Fisher-Rao distance should be an important tool for studying the non-local geometry of neural representations. Such distances should be useful for quantifying the similarities and super-threshold dissimilarities across networks. The Fisher-Rao distance has seldom been used for this purpose. Similarity metrics that are not grounded in Riemannian geometry (e.g. KL divergence) [31] and optimal transport (e.g. Wasserstein) distances [59, 39] are more typically used in this area. However, features that maximize pairwise Wasserstein distances or symmetric KL divergences yield poorer classification performance than SQFA features (see Appendix A.2). Thus, a systematic understanding of the implications of using different Riemannian distances (or similarity metrics) for learning and for geometric analyses is an important direction of future work.

As tools like SQFA that make use of Fisher-Rao distance—and tight bounds to it (e.g. Calvo-Oller bound)—become more readily available, we anticipate that Fisher-Rao distances, because of their close connection to familiar statistical will find more widespread use in statistics

Given the attractive theoretical properties of Fisher-Rao distances, it is natural to ask why they are not in more widespread use in statistics, machine learning, and neuroscience. One possible reason is that, compared to other measures of dissimilarity between probability distributions, there are few methods that use the Fisher-Rao distance [46]. Here, Fisher-Rao distances—and good approximations to them (e.g. Calvo-Oller bound [8])—were successfully used for dimensionality reduction, one of the most fundamental problems in statistics, with state-of-the-art performance. We hope that this information-geometric approach to dimensionality reduction will motivate and facilitate the use of Fisher-Rao distances in future research.

In conclusion, SQFA is a linear dimensionality reduction method that should find broad application in machine learning, statistics, and neuroscience. Its novel information geometric approach motivates several questions about the relationship between Fisher-Rao distances and discriminability that are of practical and theoretical interest.

References

- [1] S.-i. Amari. *Information Geometry and Its Applications*. Springer, Feb. 2016. ISBN 978-4-431-55978-8. Google-Books-ID: UkSFCwAAQBAJ.
- [2] M. Arjovsky, S. Chintala, and L. Bottou. Wasserstein Generative Adversarial Networks. In *Proceedings of the 34th International Conference on Machine Learning*, pages 214–223. PMLR, July 2017. URL <https://proceedings.mlr.press/v70/arjovsky17a.html>. ISSN: 2640-3498.
- [3] V. Arsigny, P. Fillard, X. Pennec, and N. Ayache. Log-Euclidean metrics for fast and simple calculus on diffusion tensors. *Magnetic Resonance in Medicine*, 56(2):411–421, 2006. ISSN 1522-2594. doi: 10.1002/mrm.20965. URL <https://onlinelibrary.wiley.com/doi/abs/10.1002/mrm.20965>. _eprint: <https://onlinelibrary.wiley.com/doi/pdf/10.1002/mrm.20965>.
- [4] G. Arvanitidis, M. González-Duque, A. Pouplin, D. Kalatzis, and S. Hauberg. Pulling back information geometry. In *Proceedings of the 25th International Conference on Artificial Intelligence and Statistics*, volume 151, Valencia, Spain, Apr. 2022. PMLR. doi: 10.48550/arXiv.2106.05367. URL <http://arxiv.org/abs/2106.05367>. arXiv:2106.05367 [cs].
- [5] C. Atkinson and A. F. S. Mitchell. Rao’s Distance Measure. *Sankhyā: The Indian Journal of Statistics, Series A (1961-2002)*, 43(3):345–365, 1981. ISSN 0581-572X. URL <https://www.jstor.org/stable/25050283>. Publisher: Springer.
- [6] J. Burge. Image-Computable Ideal Observers for Tasks with Natural Stimuli. *Annual Review of Vision Science*, 6(1):491–517, 2020. doi: 10.1146/annurev-vision-030320-041134. URL <https://doi.org/10.1146/annurev-vision-030320-041134>. _eprint: <https://doi.org/10.1146/annurev-vision-030320-041134>.
- [7] J. Burge and W. S. Geisler. Optimal speed estimation in natural image movies predicts human performance. *Nature Communications*, 6(1):7900, Aug. 2015. ISSN 2041-1723. doi: 10.1038/ncomms8900. URL <https://www.nature.com/articles/ncomms8900>. Publisher: Nature Publishing Group.
- [8] M. Calvo and J. M. Oller. A distance between multivariate normal distributions based in an embedding into the siegel group. *Journal of Multivariate Analysis*, 35(2):223–242, Nov. 1990. ISSN 0047-259X. doi: 10.1016/0047-259X(90)90026-E. URL <https://www.sciencedirect.com/science/article/pii/0047259X9090026E>.
- [9] M. Calvo and J. M. Oller. A distance between elliptical distributions based in an embedding into the Siegel group. *Journal of Computational and Applied Mathematics*, 145(2):319–334, Aug. 2002. ISSN 0377-0427. doi: 10.1016/S0377-0427(01)00584-2. URL <https://www.sciencedirect.com/science/article/pii/S0377042701005842>.
- [10] B. M. Chin and J. Burge. Predicting the Partition of Behavioral Variability in Speed Perception with Naturalistic Stimuli. *The Journal of Neuroscience*, 40(4):864–879, Jan. 2020. ISSN 0270-6474, 1529-2401. doi: 10.1523/JNEUROSCI.1904-19.2019. URL <https://www.jneurosci.org/lookup/doi/10.1523/JNEUROSCI.1904-19.2019>.
- [11] E. Choi and C. Lee. Feature extraction based on the Bhattacharyya distance. *Pattern Recognition*, 36(8):1703–1709, Aug. 2003. ISSN 0031-3203. doi: 10.1016/S0031-3203(03)00035-9. URL <https://www.sciencedirect.com/science/article/pii/S0031320303000359>.
- [12] S. Chung and L. F. Abbott. Neural population geometry: An approach for understanding biological and artificial neural networks. *Current Opinion in Neurobiology*, 70:137–144, Oct. 2021. ISSN 0959-4388. doi: 10.1016/j.conb.2021.10.010. URL <https://www.sciencedirect.com/science/article/pii/S0959438821001227>.
- [13] M. Congedo and S. Jain. A Julia Package for manipulating Brain-Computer Interface Data in the Manifold of Positive Definite Matrices. In *2019 IEEE International Conference on Systems, Man and Cybernetics (SMC)*, pages 211–216, Bari, Italy, Oct. 2019. IEEE. ISBN 978-1-72814-569-3. doi: 10.1109/SMC.2019.8914223. URL <https://ieeexplore.ieee.org/document/8914223/>.

- [14] M. Congedo, P. Rodrigues, F. Bouchard, A. Barachant, and C. Jutten. A closed-form unsupervised geometry-aware dimensionality reduction method in the Riemannian Manifold of SPD matrices. In *2017 39th Annual International Conference of the IEEE Engineering in Medicine and Biology Society (EMBC)*, pages 3198–3201, July 2017. doi: 10.1109/EMBC.2017.8037537. URL <https://ieeexplore.ieee.org/document/8037537/?arnumber=8037537>. ISSN: 1558-4615.
- [15] S. I. R. Costa, S. A. Santos, and J. E. Strapasson. Fisher information distance: A geometrical reading. *Discrete Applied Mathematics*, 197:59–69, Dec. 2015. ISSN 0166-218X. doi: 10.1016/j.dam.2014.10.004. URL <https://www.sciencedirect.com/science/article/pii/S0166218X14004211>.
- [16] J. P. Cunningham and Z. Ghahramani. Linear Dimensionality Reduction: Survey, Insights, and Generalizations. *Journal of Machine Learning Research*, 16:2859–2900, 2015.
- [17] P. Dayan and L. F. Abbott. *Theoretical Neuroscience: Computational and Mathematical Modeling of Neural Systems*. MIT Press, Aug. 2005. ISBN 978-0-262-54185-5. Google-Books-ID: fLT4DwAAQBAJ.
- [18] X. Ding, D. Lee, J. Melander, G. Sivulka, S. Ganguli, and S. Baccus. Information Geometry of the Retinal Representation Manifold. *Advances in Neural Information Processing Systems*, 36:44310–44322, Dec. 2023. URL https://proceedings.neurips.cc/paper_files/paper/2023/hash/8a267516a7a697965c6ae4f48b908605-Abstract-Conference.html.
- [19] R. Duin and M. Loog. Linear dimensionality reduction via a heteroscedastic extension of LDA: the Chernoff criterion. *IEEE Transactions on Pattern Analysis and Machine Intelligence*, 26(6):732–739, June 2004. ISSN 1939-3539. doi: 10.1109/TPAMI.2004.13. URL <https://ieeexplore.ieee.org/document/1288523/?arnumber=1288523>. Conference Name: IEEE Transactions on Pattern Analysis and Machine Intelligence.
- [20] A. Dwivedi, S. Wang, and A. Tajer. Discriminant Analysis under f-Divergence Measures. *Entropy*, 24(2):188, Feb. 2022. ISSN 1099-4300. doi: 10.3390/e24020188. URL <https://www.mdpi.com/1099-4300/24/2/188>. Number: 2 Publisher: Multidisciplinary Digital Publishing Institute.
- [21] J. Feather, D. Lipshutz, S. E. Harvey, A. H. Williams, and E. P. Simoncelli. Discriminating image representations with principal distortions, Oct. 2024. URL <http://arxiv.org/abs/2410.15433>. arXiv:2410.15433 [q-bio].
- [22] R. Flamary, M. Cuturi, N. Courty, and A. Rakotomamonjy. Wasserstein Discriminant Analysis. *Machine Learning*, 107(12):1923–1945, Dec. 2018. ISSN 0885-6125, 1573-0565. doi: 10.1007/s10994-018-5717-1. URL <http://arxiv.org/abs/1608.08063>. arXiv:1608.08063 [cs, stat].
- [23] K. Fukunaga. *Introduction to Statistical Pattern Recognition*. Academic Press, second edition, 1990. ISBN 978-0-08-047865-4. Google-Books-ID: BIJZTGjTxBgC.
- [24] M. T. Harandi, M. Salzmann, and R. Hartley. From Manifold to Manifold: Geometry-aware Dimensionality Reduction for SPD Matrices. In *Computer Vision – ECCV 2014*, volume 8690, pages 17–32, Cham, 2014. Springer International Publishing. ISBN 978-3-319-10604-5 978-3-319-10605-2. doi: https://doi.org/10.1007/978-3-319-10605-2_2. URL http://link.springer.com/10.1007/978-3-319-10605-2_2.
- [25] S. E. Harvey, B. W. Larsen, and A. H. Williams. Duality of Bures and Shape Distances with Implications for Comparing Neural Representations. In *Proceedings of UniReps: the First Workshop on Unifying Representations in Neural Models*, pages 11–26. PMLR, May 2024. URL <https://proceedings.mlr.press/v243/harvey24a.html>. ISSN: 2640-3498.
- [26] D. Herrera-Esposito and J. Burge. Optimal motion-in-depth estimation with natural stimuli, Mar. 2024. URL <https://www.biorxiv.org/content/10.1101/2024.03.14.585059v1>. Pages: 2024.03.14.585059 Section: New Results.

- [27] Z. Huang, R. Wang, S. Shan, X. Li, and X. Chen. Log-Euclidean Metric Learning on Symmetric Positive Definite Manifold with Application to Image Set Classification. In *Proceedings of the 32nd International Conference on Machine Learning*, pages 720–729. PMLR, June 2015. URL <https://proceedings.mlr.press/v37/huanga15.html>. ISSN: 1938-7228.
- [28] P. Jaini and J. Burge. Linking normative models of natural tasks to descriptive models of neural response. *Journal of Vision*, 17(12):16, Oct. 2017. ISSN 1534-7362. doi: 10.1167/17.12.16. URL <https://doi.org/10.1167/17.12.16>.
- [29] N. Karampatziakis and P. Mineiro. Discriminative Features via Generalized Eigenvectors. *International conference on machine learning*, 2014.
- [30] A. Kohn, R. Coen-Cagli, I. Kanitscheider, and A. Pouget. Correlations and Neuronal Population Information. *Annual Review of Neuroscience*, 39(1):237–256, 2016. doi: 10.1146/annurev-neuro-070815-013851. URL <https://doi.org/10.1146/annurev-neuro-070815-013851>. eprint: <https://doi.org/10.1146/annurev-neuro-070815-013851>.
- [31] N. Kriegeskorte and X.-X. Wei. Neural tuning and representational geometry. *Nature Reviews Neuroscience*, 22(11):703–718, Nov. 2021. ISSN 1471-0048. doi: 10.1038/s41583-021-00502-3. URL <https://www.nature.com/articles/s41583-021-00502-3>. Publisher: Nature Publishing Group.
- [32] Y. LeCun, Y. Bengio, and G. Hinton. Deep learning. *Nature*, 521(7553):436–444, May 2015. ISSN 1476-4687. doi: 10.1038/nature14539. URL <https://www.nature.com/articles/nature14539>. Publisher: Nature Publishing Group.
- [33] T. Liang, T. Poggio, A. Rakhlin, and J. Stokes. Fisher-Rao Metric, Geometry, and Complexity of Neural Networks. In *Proceedings of the Twenty-Second International Conference on Artificial Intelligence and Statistics*, pages 888–896. PMLR, Apr. 2019. URL <https://proceedings.mlr.press/v89/liang19a.html>. ISSN: 2640-3498.
- [34] M. Loog, R. Duin, and R. Haeb-Umbach. Multiclass linear dimension reduction by weighted pairwise Fisher criteria. *IEEE Transactions on Pattern Analysis and Machine Intelligence*, 23(7):762–766, July 2001. ISSN 1939-3539. doi: 10.1109/34.935849. URL <https://ieeexplore.ieee.org/abstract/document/935849>. Conference Name: IEEE Transactions on Pattern Analysis and Machine Intelligence.
- [35] N. Maheswaranathan, L. T. McIntosh, H. Tanaka, S. Grant, D. B. Kastner, J. B. Melander, A. Nayeibi, L. E. Brezovec, J. H. Wang, S. Ganguli, and S. A. Baccus. Interpreting the retinal neural code for natural scenes: From computations to neurons. *Neuron*, 111(17):2742–2755.e4, Sept. 2023. ISSN 08966273. doi: 10.1016/j.neuron.2023.06.007. URL <https://linkinghub.elsevier.com/retrieve/pii/S0896627323004671>.
- [36] H. K. Miyamoto, F. C. C. Meneghetti, J. Pinele, and S. I. R. Costa. On closed-form expressions for the Fisher–Rao distance. *Information Geometry*, 7(2):311–354, Nov. 2024. ISSN 2511-249X. doi: 10.1007/s41884-024-00143-2. URL <https://doi.org/10.1007/s41884-024-00143-2>.
- [37] R. Moreno-Bote, J. Beck, I. Kanitscheider, X. Pitkow, P. Latham, and A. Pouget. Information-limiting correlations. *Nature Neuroscience*, 17(10):1410–1417, Oct. 2014. ISSN 1546-1726. doi: 10.1038/nn.3807. URL <https://www.nature.com/articles/nn.3807>. Number: 10 Publisher: Nature Publishing Group.
- [38] J. A. Movshon, I. D. Thompson, and D. J. Tolhurst. Spatial and temporal contrast sensitivity of neurones in areas 17 and 18 of the cat’s visual cortex. *The Journal of Physiology*, 283(1):101–120, 1978. ISSN 1469-7793. doi: 10.1113/jphysiol.1978.sp012490. URL <https://onlinelibrary.wiley.com/doi/abs/10.1113/jphysiol.1978.sp012490>.
- [39] A. Nejatbakhsh, I. Garon, and A. Williams. Estimating Noise Correlations Across Continuous Conditions With Wishart Processes. *Advances in Neural Information Processing Systems*, 36:54032–54045, Dec. 2023. URL https://proceedings.neurips.cc/paper_files/paper/2023/hash/a935ba2236c6ba0fb620f23354e789ff-Abstract-Conference.html.

- [40] L. Ni and J. Burge. Feature-specific divisive normalization improves natural image encoding for depth perception, Sept. 2024. URL <http://biorxiv.org/lookup/doi/10.1101/2024.09.05.611536>.
- [41] F. Nielsen. An Elementary Introduction to Information Geometry. *Entropy*, 22(10):1100, Oct. 2020. ISSN 1099-4300. doi: 10.3390/e22101100. URL <https://www.mdpi.com/1099-4300/22/10/1100>. Number: 10 Publisher: Multidisciplinary Digital Publishing Institute.
- [42] F. Nielsen. A Simple Approximation Method for the Fisher–Rao Distance between Multivariate Normal Distributions. *Entropy*, 25(4):654, Apr. 2023. ISSN 1099-4300. doi: 10.3390/e25040654. URL <https://www.mdpi.com/1099-4300/25/4/654>. Number: 4 Publisher: Multidisciplinary Digital Publishing Institute.
- [43] F. Nielsen and A. Soen. pyBregMan: A Python library for Bregman Manifolds, Aug. 2024. URL <http://arxiv.org/abs/2408.04175>. arXiv:2408.04175 [cs].
- [44] T. Parr, L. Da Costa, and K. Friston. Markov blankets, information geometry and stochastic thermodynamics. *Philosophical Transactions of the Royal Society A: Mathematical, Physical and Engineering Sciences*, 378(2164):20190159, Dec. 2019. doi: 10.1098/rsta.2019.0159. URL <https://royalsocietypublishing.org/doi/full/10.1098/rsta.2019.0159>. Publisher: Royal Society.
- [45] F. Pedregosa, G. Varoquaux, A. Gramfort, V. Michel, B. Thirion, O. Grisel, M. Blondel, P. Prettenhofer, R. Weiss, V. Dubourg, J. Vanderplas, A. Passos, and D. Cournapeau. Scikit-learn: Machine Learning in Python. *Journal of Machine Learning Research*, 12:2825–2830, 2011.
- [46] J. Pinele, J. E. Strapasson, and S. I. R. Costa. The Fisher–Rao Distance between Multivariate Normal Distributions: Special Cases, Bounds and Applications. *Entropy*, 22(4):404, Apr. 2020. ISSN 1099-4300. doi: 10.3390/e22040404. URL <https://www.mdpi.com/1099-4300/22/4/404>. Number: 4 Publisher: Multidisciplinary Digital Publishing Institute.
- [47] N. J. Priebe, S. G. Lisberger, and J. A. Movshon. Tuning for Spatiotemporal Frequency and Speed in Directionally Selective Neurons of Macaque Striate Cortex. *Journal of Neuroscience*, 26(11):2941–2950, Mar. 2006. ISSN 0270-6474, 1529-2401. doi: 10.1523/JNEUROSCI.3936-05.2006. URL <https://www.jneurosci.org/content/26/11/2941>. Publisher: Society for Neuroscience Section: Articles.
- [48] L. Rueda and M. Herrera. Linear dimensionality reduction by maximizing the Chernoff distance in the transformed space. *Pattern Recognition*, 41(10):3138–3152, Oct. 2008. ISSN 0031-3203. doi: 10.1016/j.patcog.2008.01.016. URL <https://www.sciencedirect.com/science/article/pii/S003132030800037X>.
- [49] N. C. Rust, O. Schwartz, J. A. Movshon, and E. P. Simoncelli. Spatiotemporal Elements of Macaque V1 Receptive Fields. *Neuron*, 46(6):945–956, June 2005. ISSN 0896-6273. doi: 10.1016/j.neuron.2005.05.021. URL <https://www.sciencedirect.com/science/article/pii/S089662730500468X>.
- [50] T. Sainburg, L. McInnes, and T. Q. Gentner. Parametric UMAP Embeddings for Representation and Semisupervised Learning. *Neural Computation*, pages 1–27, Aug. 2021. ISSN 0899-7667, 1530-888X. doi: 10.1162/neco_a_01434. URL https://direct.mit.edu/neco/article/doi/10.1162/neco_a_01434/107068/Parametric-UMAP-Embeddings-for-Representation-and.
- [51] M. Thangavelu and R. Raich. Multiclass linear dimension reduction via a generalized Chernoff bound. In *2008 IEEE Workshop on Machine Learning for Signal Processing*, pages 350–355, Oct. 2008. doi: 10.1109/MLSP.2008.4685505. URL <https://ieeexplore.ieee.org/abstract/document/4685505>. ISSN: 2378-928X.
- [52] Y. Thanwerdas and X. Pennec. $O(n)$ -invariant Riemannian metrics on SPD matrices. *Linear Algebra and its Applications*, 661:163–201, Mar. 2023. ISSN 0024-3795. doi: 10.1016/j.laa.2022.12.009. URL <https://www.sciencedirect.com/science/article/pii/S0024379522004360>.

- [53] J. Vacher and P. Mamassian. Perceptual Scales Predicted by Fisher Information Metrics, Mar. 2024. URL <http://arxiv.org/abs/2310.11759>. arXiv:2310.11759 [q-bio].
- [54] J. J. Vastola, Z. Cohen, and J. Drugowitsch. Is the information geometry of probabilistic population codes learnable? In *Proceedings of the 1st NeurIPS Workshop on Symmetry and Geometry in Neural Representations*, pages 258–277. PMLR, Feb. 2023. URL <https://proceedings.mlr.press/v197/vastola23a.html>. ISSN: 2640-3498.
- [55] W. d. Vazelhes, C. J. Carey, Y. Tang, N. Vauquier, and A. Bellet. metric-learn: Metric Learning Algorithms in Python. *Journal of Machine Learning Research*, 21(138):1–6, 2020. ISSN 1533-7928. URL <http://jmlr.org/papers/v21/19-678.html>.
- [56] B. Wang and C. R. Ponce. The Geometry of Deep Generative Image Models and its Applications, Mar. 2021. URL <http://arxiv.org/abs/2101.06006>. arXiv:2101.06006 [cs, math].
- [57] X.-X. Wei and A. A. Stocker. Lawful relation between perceptual bias and discriminability. *Proceedings of the National Academy of Sciences*, 114(38):10244–10249, Sept. 2017. ISSN 0027-8424, 1091-6490. doi: 10.1073/pnas.1619153114. URL <https://pnas.org/doi/full/10.1073/pnas.1619153114>.
- [58] K. Q. Weinberger and L. K. Saul. Distance Metric Learning for Large Margin Nearest Neighbor Classification. *Journal of Machine Learning Research*, 10:207–244, 2009.
- [59] A. H. Williams, E. Kunz, S. Kornblith, and S. Linderman. Generalized Shape Metrics on Neural Representations. In *Advances in Neural Information Processing Systems*, volume 34, pages 4738–4750. Curran Associates, Inc., 2021. URL <https://proceedings.neurips.cc/paper/2021/hash/252a3dbaeb32e7690242ad3b556e626b-Abstract.html>.
- [60] Z. Ye and R. Wessel. Speed modulations in grid cell information geometry, Sept. 2024. URL <https://www.biorxiv.org/content/10.1101/2024.09.18.613797v1>. Pages: 2024.09.18.613797 Section: New Results.
- [61] J. Zhou, L. R. Duong, and E. P. Simoncelli. A unified framework for perceived magnitude and discriminability of sensory stimuli. *Proceedings of the National Academy of Sciences*, 121(25): e2312293121, June 2024. doi: 10.1073/pnas.2312293121. URL <https://www.pnas.org/doi/abs/10.1073/pnas.2312293121>. Publisher: Proceedings of the National Academy of Sciences.

A Fisher-Rao distance and discriminability in the zero-mean Gaussian case

In the main text we argue that the Fisher-Rao distance is a good proxy for discriminability because it can be interpreted as the accumulated discriminability of the infinitesimal perturbations turning one distribution into another along the geodesic (Section 2.1). Furthermore, we showed that maximizing the Fisher-Rao distance leads to features that allow for quadratic classification comparable to the state-of-the-art method for maximizing quadratic discriminability, BDM, providing further empirical evidence for the usefulness of Fisher-Rao distances as a proxy for discriminability.

However, some questions remain. For example, are there other theoretical reasons why Fisher-Rao distances are or are not a good proxy for discriminability? Do other distances between probability distributions perform as well? How well does the Fisher-Rao distance approximate the discriminability between distributions? To provide a more complete answer to these questions, in this section we further analyze Fisher-Rao distances in the case of zero-mean class-conditional distributions, for which there is an exact closed-form expression given by Equation 6,

A.1 Generalized eigenvalues reflect quadratic differences between classes

As described in the main text, the Fisher-Rao distance between two zero-mean Gaussian distributions $\mathcal{N}(0, \Psi_i)$ and $\mathcal{N}(0, \Psi_j)$ is given (up to a factor of $\sqrt{2}$) by the affine-invariant distance in $\text{SPD}(m)$

$$d_{FR}(\Psi_i, \Psi_j) = \frac{1}{\sqrt{2}} \sqrt{\sum_{k=1}^m \log^2(\lambda_k)} \quad (6)$$

where λ_k are the generalized eigenvalues of the pair of matrices (Ψ_i, Ψ_j) .

The generalized eigenvalues λ_k and generalized eigenvectors \mathbf{v}_k of the pair of matrices $\mathbf{A} \in \text{SPD}(m)$ and $\mathbf{B} \in \text{SPD}(m)$ are the solutions to the generalized eigenvalue problem $\mathbf{A}\mathbf{v}_k = \lambda_k\mathbf{B}\mathbf{v}_k$. The solution to the problem is given by the eigenvalues and eigenvectors of $\mathbf{B}^{-1/2}\mathbf{A}\mathbf{B}^{-1/2}$, where $\mathbf{B}^{-1/2}$ is the inverse square root of \mathbf{B} . If \mathbf{A} and \mathbf{B} are identical, $\mathbf{B}^{-1/2}\mathbf{A}\mathbf{B}^{-1/2}$ is the identity matrix, all the eigenvalues are 1, and $d_{FR}(\mathbf{A}, \mathbf{B}) = 0$. The farther the λ_k are from 1, the more different the matrices \mathbf{A} and \mathbf{B} are (i.e. the more different $\mathbf{B}^{-1/2}\mathbf{A}\mathbf{B}^{-1/2}$ is from the identity matrix).

Consider a random variable $\mathbf{z} \in \mathbb{R}^m$ that belongs to one of two classes i, j , with second moment matrices $\Psi_i = \mathbb{E}[\mathbf{z}\mathbf{z}^T | y = i]$ and $\Psi_j = \mathbb{E}[\mathbf{z}\mathbf{z}^T | y = j]$. Next, consider a vector $\mathbf{w} \in \mathbb{R}^m$ and the squared projection of \mathbf{z} onto \mathbf{w} , $(\mathbf{w}^T \mathbf{z})^2$. The following ratio relates to how different the squared projections are for the two classes, which is a useful proxy for quadratic discriminability:

$$R(\mathbf{w}) = \frac{\mathbb{E}[(\mathbf{w}^T \mathbf{z})^2 | y = i]}{\mathbb{E}[(\mathbf{w}^T \mathbf{z})^2 | y = j]} = \frac{\mathbf{w}^T \Psi_i \mathbf{w}}{\mathbf{w}^T \Psi_j \mathbf{w}} \quad (7)$$

The local extrema of the ratio $R(\mathbf{w})$ are obtained at the generalized eigenvectors $\mathbf{w} = \mathbf{v}_k$ of (Ψ_i, Ψ_j) , where the ratio $R(\mathbf{v}_k) = \lambda_k$ [23].

The more different λ_k is from 1, the more different are the expected squared projections $(\mathbf{v}_k^T \mathbf{z})^2$ for the two classes. Obviously, the magnitude of $\log^2 \lambda_k$ indicates how different the ratio in Equation 7 is from 1, in proportional terms. The set of \mathbf{v}_k 's spans the space of \mathbf{z} , so $d_{FR}(\Psi_i, \Psi_j)$ summarizes the quadratic differences between the classes i, j along all directions in the feature space, thus relating to the quadratic discriminability of the classes.

Of course, the quadratic discriminability between the classes depends on other factors than the ratio of the expected values of the squared projections, and larger differences in this ratio do not strictly indicate higher discriminability. However, empirical studies show that the generalized eigenvalues tend to be a good indicator of quadratic discriminability in real world datasets [29].

A.2 Empirical comparison of Fisher-Rao distance to other distances

We showed in the main text that maximizing the Fisher-Rao distance leads to good quadratic discriminability. It is unclear however whether this observation is specific to the Fisher-Rao distance, or whether it can be achieved with any distance between probability distributions. To answer this, we compare the Fisher-Rao distance to other common distances for the case of zero-mean Gaussian distributions.

A.2.1 Alternative distances and dissimilarity measures

Because zero-mean Gaussian distributions are completely characterized by their second-moment matrices, any distance in $\text{SPD}(m)$ can be used as a distance between a pair of zero-mean Gaussian distributions. There are a number of distances in $\text{SPD}(m)$ that are commonly used in the literature ([13, 52]). Here we will consider four $\text{SPD}(m)$ distances: the Bures-Wasserstein distance (and a normalized version of this distance), the Log-Euclidean distance and the Euclidean distance.

The Bures-Wasserstein distance between two matrices Ψ_i and Ψ_j in $\text{SPD}(m)$ is given by

$$d_{BW}(\Psi_i, \Psi_j) = \sqrt{\text{Tr}(\Psi_i) + \text{Tr}(\Psi_j) - 2\text{Tr}\left(\left[\Psi_i^{1/2}\Psi_j\Psi_i^{1/2}\right]^{1/2}\right)} \quad (8)$$

The Bures-Wasserstein distance is equivalent to the optimal transport distance between the zero-mean Gaussians $\mathcal{N}(0, \Psi_i)$ and $\mathcal{N}(0, \Psi_j)$ [52]. The earth-mover's intuition of the optimal transport distance is that it measures how much work it takes to move a pile of dirt shaped like $\mathcal{N}(0, \Psi_i)$ to a pile of dirt shaped like $\mathcal{N}(0, \Psi_j)$. This distance is commonly used in machine learning, statistics and neuroscience [2, 22, 25]. However, it is not invariant to invertible linear transformations like the affine-invariant distance, and its metric is not as closely related to discriminability as the Fisher information metric.

Because the Bures-Wasserstein distance is not invariant to scalings of the data space, we also consider a normalized version of the Bures-Wasserstein distance, to emphasize differences between the distributions that are less sensitive to the overall scale. The normalized Bures-Wasserstein distance is given by

$$d_{BWN}(\Psi_i, \Psi_j) = \frac{d_{BW}(\Psi_i, \Psi_j)}{\sqrt{\text{Tr}(\Psi_i) + \text{Tr}(\Psi_j)}} \quad (9)$$

The Log-Euclidean distance is given by

$$d_{LE}(\Psi_i, \Psi_j) = \|\log(\Psi_i) - \log(\Psi_j)\|_F \quad (10)$$

The Log-Euclidean distance is popular because it is a simple and computationally efficient way to measure distances in $\text{SPD}(m)$ [27]. The Log-Euclidean distance is also a good approximation to the affine-invariant distance when the matrices are close to the identity matrix [3, 27, 13].

The Euclidean distance is given by

$$d_E(\Psi_i, \Psi_j) = \|\Psi_i - \Psi_j\|_F \quad (11)$$

The Euclidean distance is rarely used in practice for SPD matrices because it does not take into account the geometry of $\text{SPD}(m)$.

We also consider two common measures of dissimilarity between probability distributions that are not distances, but that are related to discriminability. These are the symmetric Kullback-Leibler (KL) divergence (or Jeffreys divergence) and the Bhattacharyya distance.

The symmetric KL divergence, or Jeffreys divergence between zero-mean Gaussians $\mathcal{N}(0, \Psi_i)$ and $\mathcal{N}(0, \Psi_j)$ is given by

$$d_{KL}(\Psi_i, \Psi_j) = \frac{\text{KL}(\Psi_i, \Psi_j) + \text{KL}(\Psi_j, \Psi_i)}{2} \quad (12)$$

where $\text{KL}(\Psi_i, \Psi_j) = \frac{1}{2} \left(\text{Tr}(\Psi_j^{-1}\Psi_i) + \log \frac{\det(\Psi_j)}{\det(\Psi_i)} - m \right)$ is the KL divergence between $\mathcal{N}(0, \Psi_i)$ and $\mathcal{N}(0, \Psi_j)$. The KL divergence between two distributions is a measure of how different the two distributions are, and it is commonly used in statistics and machine learning, although it is not symmetric. The Jeffreys divergence is a symmetric version of the KL divergence.

Following Equation 5, the Bhattacharyya distance between two zero-mean Gaussians is given by

$$d_{Bhatt}(\Psi_i, \Psi_j) = \frac{1}{2} \log \left(\frac{\det\left(\frac{\Psi_i + \Psi_j}{2}\right)}{\sqrt{\det \Psi_i \det \Psi_j}} \right) = \sum_{k=1}^m \log \left(\frac{1 + \lambda_k}{2} \right) - \frac{1}{2} \log \lambda_k \quad (13)$$

where λ_k is the k -th generalized eigenvalue of (Ψ_i, Ψ_j) . The second equality is obtained by using the generalized eigenvectors to simultaneously diagonalize the matrices Ψ_i and Ψ_j [23], using the

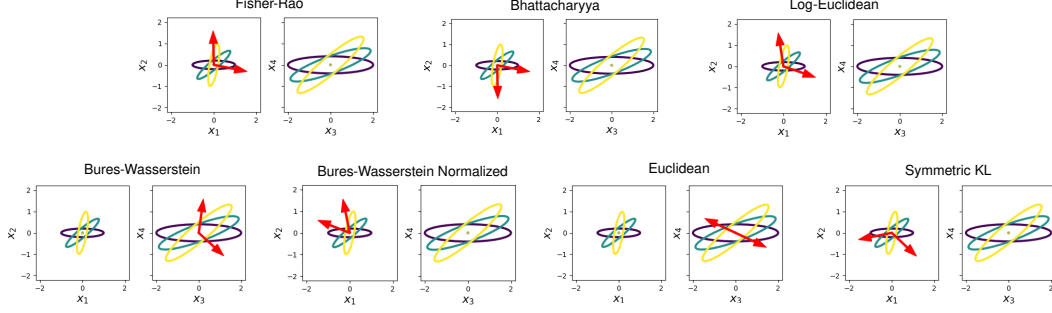


Figure 6: Toy problem evaluation of different distances. We learned 2 filters in the full four-dimensional data space using different distances for the smSQFA objective. Each panel shows a pair of the dimensions of the data space. The ellipses show the distributions of the three classes, with the class indicated by color. The filters learned are shown as arrows overlayed on the data. The distance used to learn the filters is indicated in the title of each panel.

equivalence of the determinant to the the product of the, and the properties of the logarithm. Like the affine-invariant distance, the Bhattacharyya distance is invariant to invertible linear transformations, and it is a function of the generalized eigenvalues of the pair of matrices (Ψ_i, Ψ_j) .

A.2.2 Comparison of distances in toy problem

To compare the distances, we designed a toy problem with three classes in four dimensions (Figure 6). The classes have zero mean and different covariance matrices. The covariance matrices are obtained by taking one covariance matrix and rotating it by different angles. Dimensions 1-2 have smaller variance, but larger rotation between classes, making them more discriminative. Dimensions 3-4 have larger variance but smaller rotation, making them less discriminative.

As expected, the filters learned using the Fisher-Rao distance are selective for dimensions 1-2, which are the most discriminative (Figure 6). The filters learned using the Bhattacharyya distance are also selective for dimensions 1-2, which is not surprising since this is a well-known distance for learning features that are useful for quadratic classification. The filters learned with the symmetric KL divergence are also selective for dimensions 1-2. Also, the filters learned using the Log-Euclidean distance are selective for dimensions 1-2. This is not surprising considering that the Log-Euclidean geometry is similar to the affine-invariant (i.e. Fisher-Rao) geometry (at least close to the identity matrix) [27, 3].

The filters learned using the Bures-Wasserstein, Euclidean are selective for dimensions 3-4. For the Bures-Wasserstein distance, this can be explained using the earth-mover’s intuition: the effort to move the dirt piles increases with the scale of the Gaussians. Thus, for the goal of learning features that maximize second-order discriminability, the Bures-Wasserstein distance is not as useful as the affine-invariant distance. Nonetheless, the normalized Bures-Wasserstein distance does select for dimensions 1-2.

A.2.3 Comparison of distances in real-world datasets

Next, we compared the distances using the two datasets of the main text where discriminability was mainly based on second-order statistics: the SVHN dataset and the speed estimation dataset. smSQFA and the zero-mean Gaussian assumption are particularly suitable for these datasets. Like in the main text, we learned 9 filters by using each distance to maximize the smSQFA objective. We tested the accuracy of a QDA classifier using each set of learned features.

A similar pattern of performance was observed across the two tasks (Figure 7). In both cases, the Fisher-Rao distance and the Log-Euclidean distance have the highest accuracy, closely followed by the Bhattacharyya distance and the symmetric KL divergence. The Bures-Wasserstein distance performed poorly, only outperforming the Euclidean distance. The normalized Bures-Wasserstein distance performed better than the Bures-Wasserstein distance, but worse than most other distances.

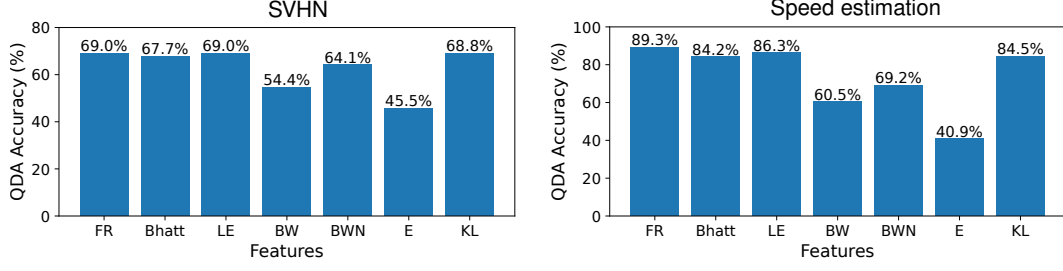


Figure 7: Accuracy of a QDA classifier using features learned by maximizing different distances and dissimilarity measures. 9 filters were learned for each distance. **Left.** SVHN dataset. **Right.** Speed estimation dataset. The distances are labeled as FR (Fisher-Rao), Bhatt (Bhattacharyya), LE (Log-Euclidean), BW (Bures-Wasserstein), BWN (Bures-Wasserstein Normalized), E (Euclidean), and KL (symmetric Kullback-Leibler).

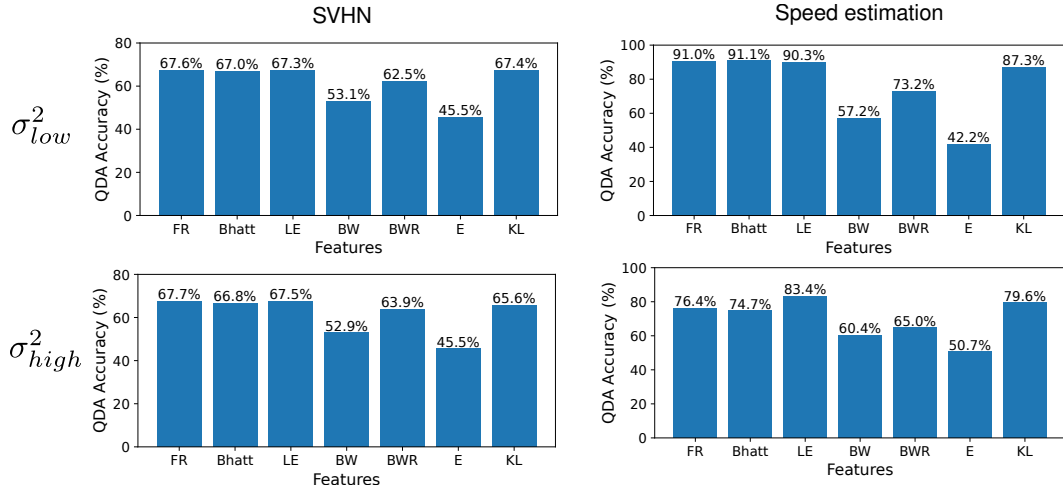


Figure 8: Effect of regularization noise on the performance of different distances. The top row shows the QDA accuracy for the features learned with low noise. The bottom row shows the QDA accuracy for the features learned with high noise. **Left.** SVHN dataset. **Right.** Speed estimation dataset.

This result suggests that while serving as a proxy for discriminability like the Fisher-Rao distance is not a general property of all distances, other distances and dissimilarity measures can also be reasonable proxies for discriminability in feature learning.

Next, we explored how robust this result is to the regularization noise, and the violation of the zero-mean Gaussian assumption. First, we repeated the analysis above, but using different values for the added regularization noise σ^2 during training. The same value is shared for all distances. Specifically, denoting by σ^2 the level of noise used in the analysis above (as reported in the main text), we tested $\sigma_{low}^2 = 0.25\sigma^2$ and $\sigma_{high}^2 = 4\sigma^2$.

We observed that some broad patterns remain the same across the different noise levels (Figure 8). The Fisher-Rao distance allowed for good performance, higher than other distances in most cases. In one case, however, the Log-Euclidean and the symmetric KL divergence performed better. Thus, across six different conditions (two datasets and three noise levels), the Fisher-Rao distance was the best performer (or tied for the best performer) in five cases.

The Euclidean distance remained the worst performer across conditions, followed by the Bures-Wasserstein distance. The normalized Bures-Wasserstein distance was better than the Bures-Wasserstein distance, but considerably worse than the best performers.

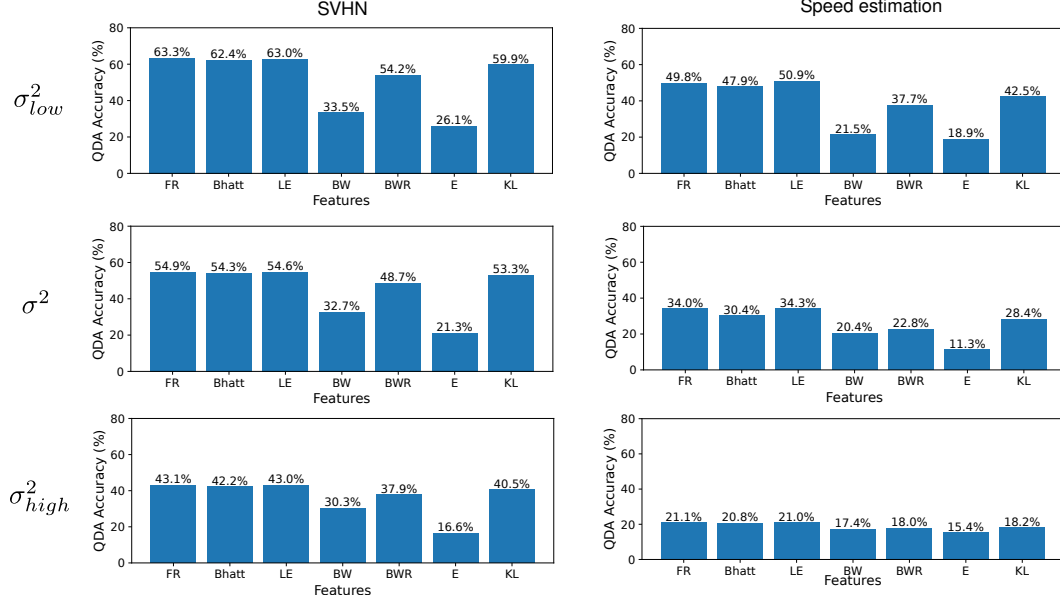


Figure 9: Gaussian data evaluation of different distances. Accuracy of the QDA classifier for the features of each distance was evaluated using synthetic Gaussian data. From top to bottom, the three rows show the results for low, medium, and high regularization noise. **Left.** SVHN dataset. **Right.** Speed estimation dataset.

Another interesting question is to what extent the performance patterns are driven by the mismatch between the class-conditional Gaussian assumption and the actual distributions of the data. That is, how would the distances perform if the Gaussian assumption was correct?

To answer this, we generated synthetic Gaussian data for testing the learned features. For the set of features learned with each distance, we computed the class-conditional second-moment matrices of the projected data, including the added regularization noise. Then we generated a synthetic testing dataset by sampling from the zero-mean Gaussian distribution with the corresponding second-moment matrix for each class. We generated 10000 samples per class for SVHN and 3000 for speed estimation. Then we tested the QDA classifier using these Gaussian-distributed samples.

Using the Gaussian-distributed testing dataset, the Fisher-Rao features performed the best in general, tied with the Log-Euclidean distance. This shows that, under the Gaussian assumption, the Fisher-Rao distance is a good proxy for discriminability, at least for the range of second-moment matrices found in these real-world datasets.

In sum, these results show that the properties of the Fisher-Rao distance make it a good proxy for discriminability in real-world datasets. The Fisher-Rao distance outperformed other well known distances and dissimilarity measures, including the Bhattacharyya distance. Interestingly, the Bures-Wasserstein distance, which is another distance that is popular in machine learning [22, 2] and neuroscience [25], performed poorly as a discriminability proxy across all examples. Other distances, however, also performed on par with the Fisher-Rao distance, particularly the Log-Euclidean distance. However, while the Fisher-Rao distance can be extended to the non-zero mean case, and to other distributions, there is no natural extension of the Log-Euclidean distance to the non-zero mean case.

It is important to note that the performance of a distance as a proxy for pairwise discriminability is not the only factor determining the performance of the final classifier on the learned features. Another essential factor is how well the sum of pairwise distances relates to the discriminability of the multi-class problem. This is a well-known issue that has been studied in the context of LDA [34]. Future work should explore the contribution of this factor to the performance of SQFA and the different dissimilarity measures.

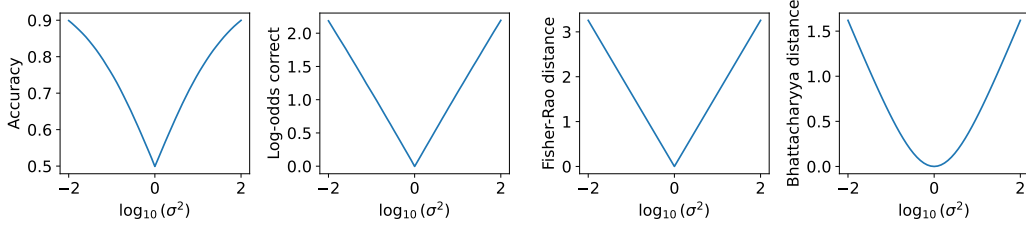


Figure 10: Distances and Bayes error for 1D Gaussian distributions. From left to right, the four panels show, as a function of $\log_{10}(\sigma^2)$, the Fisher-Rao distance, the Bhattacharyya distance, the accuracy of the Bayes classifier for two Gaussian classes, and the log-odds of a correct classification.

A.3 Fisher-Rao distance and Bayes error in 1D and 2D case

Finally, we explicitly compare the Fisher-Rao distance and the Bhattacharyya distance to the Bayes error for zero-mean Gaussians in the 1D and 2D cases.

The analysis of these quantities in the general case of pairs of arbitrary zero-mean Gaussians $\mathcal{N}(0, \Psi_i)$ and $\mathcal{N}(0, \Psi_j)$ can be reduced to the analysis of pairs of Gaussians of the form $\mathcal{N}(0, \mathbf{D})$ and $\mathcal{N}(0, \mathbf{I})$, where \mathbf{D} is a diagonal matrix with positive entries and \mathbf{I} is the identity matrix. This is because all of these quantities are invariant to invertible linear transformations of the data, and any two arbitrary SPD matrices Ψ_i and Ψ_j can be simultaneously diagonalized by a linear transformation of the data space that maps Ψ_i to a diagonal matrix \mathbf{D} and Ψ_j to \mathbf{I} .

More specifically, such simultaneous diagonalization can be obtained using the generalized eigenvectors of (Ψ_j, Ψ_i) . If the matrix \mathbf{V} contains the generalized eigenvectors of (Ψ_j, Ψ_i) as columns, then $\mathbf{V}^T \Psi_i \mathbf{V} = \mathbf{D}$ and $\mathbf{V}^T \Psi_j \mathbf{V} = \mathbf{I}$, where the diagonal elements of \mathbf{D} are the generalized eigenvalues [23]. Thus, we analyze the Fisher-Rao distance, the Bhattacharyya distance, and the Bayes error for the pair of distributions $\mathcal{N}(0, \mathbf{D})$ and $\mathcal{N}(0, \mathbf{I})$ as a function of the entries of \mathbf{D} , which exhausts all the possible cases.

We computed the Bayes error for each value of \mathbf{D} by by simulating 100000 samples from each $\mathcal{N}(0, \mathbf{D})$ and $\mathcal{N}(0, \mathbf{I})$ distribution, and then computing Bayes error (e_B) as the fraction of samples that were misclassified by a QDA classifier with the true parameters. We compute the Bayes accuracy (a_B) as $a_B = 1 - e_B$. Because the accuracy is bounded to be between 0 and 1, we also computed the log-odds of correctly classifying a sample, given by $\log\left(\frac{a_B}{e_B}\right)$. The log-odds is a common way to map probabilities onto the real line.

Zero-mean Gaussian, 1D case. In the 1D case, the matrix \mathbf{D} is a single positive number σ^2 . Figure 10 shows the Fisher-Rao distance, the Bhattacharyya distance, and the Bayes error as a function of σ^2 .

Following Equation 6, it is clear that the Fisher-Rao distance is a linear function of $|\log_{10} \sigma^2|$ in the 1D case. As can be deduced by analyzing Equation 13, the Bhattacharyya distance is approximately linear for larger values of $|\sigma^2|$, but Figure 10 shows that it is shaped like a parabola closer to 0. Interestingly, the Bayes accuracy is approximately linear for small values of σ^2 , although as expected, it begins to saturate for larger values of σ^2 . (since it is bounded by 1). Finally, the log-odds of a correct classification is linear as a function of $\log_{10} \sigma^2$.

The above results suggest that the Fisher-Rao distance is a good proxy for discriminability in the zero-mean 1D Gaussian case. Particularly at values of $\log_{10} \sigma^2$ close to 0, the Fisher-Rao distance curve has a similar shape (i.e. linear) to both the Bayes error and the log-odds of a correct classification. Thus, optimizing the Fisher-Rao distance under these conditions should lead to features that maximize discriminability. In contrast, the Bhattacharyya distance behaves quite differently from the Bayes error and the log-odds of a correct for small values of $|\log_{10} \sigma^2|$.

Zero-mean Gaussian, 2D case. Next we analyze the 2D case. Here, there are two parameters, σ_1^2 and σ_2^2 . The top row of Figure 11 shows the level sets of accuracy, the log-odds correct, the

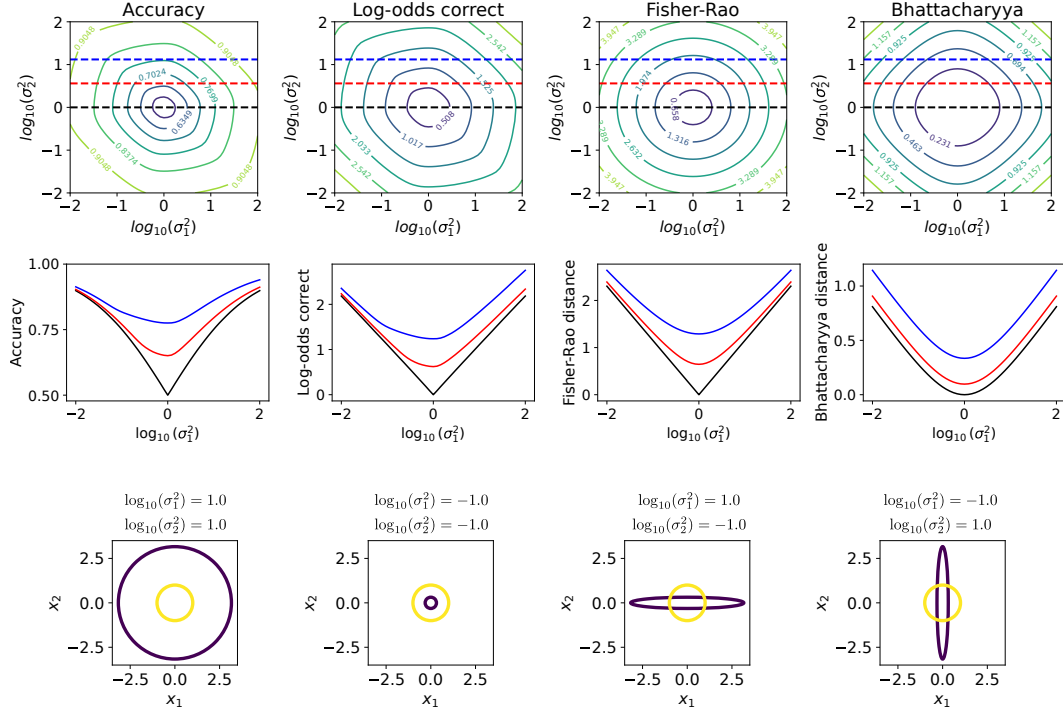


Figure 11: Distances and Bayes error for 2D Gaussian distributions. From left to right, the panels show the accuracy of the Bayes classifier for two Gaussian classes, the log-odds of a correct classification, the Fisher-Rao distance, and the Bhattacharyya distance **Top**. Contour plots of the quantities as a function of $\log_{10}(\sigma_1^2)$ and $\log_{10}(\sigma_2^2)$. The values for the contour lines are shown as a color map. The horizontal dashed lines indicate the 1D slices that are shown in the middle row. **Middle**. The same quantities as the top row, shown as a function of $\log_{10}(\sigma_1^2)$, for a fixed values of $\log_{10}(\sigma_2^2)$. The values used are 0.0 (black), 0.56 (red), and 1.12 (blue). **Bottom**. Examples of two zero-mean distributions for different values of $\log_{10} \sigma_1^2$ and $\log_{10} \sigma_2^2$.

Fisher-Rao distance, and the Bhattacharyya distance as a function of $\log_{10} \sigma_1^2$ and $\log_{10} \sigma_2^2$. The second row shows the values of the same quantities as a function of $\log_{10} \sigma_1^2$ for fixed values of $\log_{10} \sigma_2^2$, indicated by dashed lines in the top row. The bottom row shows examples of two zero-mean distributions for different values of $\log_{10} \sigma_1^2$ and $\log_{10} \sigma_2^2$.

Interestingly, we see that the level sets of the Fisher-Rao distance, the Bhattacharyya distance, and the QDA accuracy all have distinct shapes. The contours of the accuracy and log-odds correct have more circular shapes close to the origin, but acquire a tilted hexagonal shape farther from the origin. As expected from Equation 6, the Fisher-Rao countour sets are circles. Finally, the Bhattacharyya distance contours are more circular close to the origin, and acquire a rhomboidal shape farther from the origin.

These contour shapes show that the Fisher-Rao distance is not a perfect proxy for discriminability, since it does not capture the interactions between the two parameters $\log_{10} \sigma_1^2$ and $\log_{10} \sigma_2^2$ that lead to the peculiar hexagonal shape of the accuracy and log-odds correct plots. The Fisher-Rao distance provides a good approximation of the log-odds correct, however, at smaller values of $\log_{10} \sigma_1^2$ and $\log_{10} \sigma_2^2$. The Bhattacharyya distance does seem to capture some of these interactions, since some of its diagonal contours (bottom left and top right) match the hexagonal shapes, but it is not a perfect match either.

To visualize this further, we plotted the values of the distances and accuracies for three different slices of the 2D space, with fixed values of $\log_{10} \sigma_2^2$ (0.0, 0.56, 1.12). (Figure 11, middle row). For the first two slices (black and red), the Fisher-Rao distance and the log-odds correct are very similar

across the range of values of $\log_{10} \sigma_1^2$, but they become less similar for the third slice (blue), where the asymmetry of the log-odds correct is more pronounced.

In sum, this analysis shows that the Fisher-Rao distance is a good proxy for discriminability, particularly in the 1D case, and when the generalized eigenvalues are closer to 1 (i.e. when $\log_{10} \sigma^2$ is close to 0), but it is not perfect. The Bhattacharyya distance seems a worse proxy for discriminability across some of the tested conditions, but it is able to capture some patterns of accuracy that the Fisher-Rao distance does not. Thus, the efficacy of the Fisher-Rao distance as a discriminability proxy, and its performance relative to the Bhattacharyya distance will depend on the specific conditions of the data.

B LDA features maximize the Fisher-Rao squared distances between homoscedastic Gaussians

In this section, we prove that LDA maximizes the pairwise Fisher-Rao squared distances between classes in the sub-manifold of Gaussians with shared covariance matrix.

For a labeled random variable $\mathbf{x} \in \mathbb{R}^n$ with class labels $y \in \{1, \dots, c\}$, the goal of LDA is to find the filters $\mathbf{F} \in \mathbb{R}^{n \times m}$ such that the variable $\mathbf{z} = \mathbf{F}^T \mathbf{x}$ maximizes the between-class scatter relative to the within-class scatter. Mathematically, this is typically formulated as maximizing the Fisher criterion

$$\text{Tr}(\Sigma^{-1} \mathbf{S}_z) \quad (14)$$

where Σ is the residual within-class covariance matrix of the data (i.e. the covariance matrix of the data after subtracting the class mean from each data point), and \mathbf{S}_z is the between-class scatter matrix of \mathbf{z} , defined as

$$\mathbf{S}_z = \frac{1}{c} \sum_{i=1}^c (\boldsymbol{\mu}_i - \boldsymbol{\mu})(\boldsymbol{\mu}_i - \boldsymbol{\mu})^T$$

where $\boldsymbol{\mu}_i$ is the mean of class i in the feature space and $\boldsymbol{\mu} = \sum_{i=1}^c \boldsymbol{\mu}_i$.

We wish to prove that the dimensionality reduction objective in Equation 14 is equivalent to maximizing the pairwise Fisher-Rao squared distances between classes under the assumption that the classes are homoscedastic Gaussians. The Fisher-Rao distance between $\mathcal{N}(\boldsymbol{\mu}_i, \Sigma)$ and $\mathcal{N}(\boldsymbol{\mu}_j, \Sigma)$ along the submanifold of Gaussians with covariance Σ is given by [46]

$$d_{\Sigma}(\boldsymbol{\mu}_i, \boldsymbol{\mu}_j) = \sqrt{(\boldsymbol{\mu}_i - \boldsymbol{\mu}_j)^T \Sigma^{-1} (\boldsymbol{\mu}_i - \boldsymbol{\mu}_j)} \quad (15)$$

(note that this is not the same as the Fisher-Rao distance along the general manifold of Gaussian distributions). The sum of pairwise squared Fisher-Rao distances between the classes is given by

$$\frac{1}{2} \sum_{i=1}^c \sum_{j=1}^c d_{\Sigma}(\boldsymbol{\mu}_i, \boldsymbol{\mu}_j)^2 = \frac{1}{2} \sum_{i=1}^c \sum_{j=1}^c (\boldsymbol{\mu}_i - \boldsymbol{\mu}_j)^T \Sigma^{-1} (\boldsymbol{\mu}_i - \boldsymbol{\mu}_j) \quad (16)$$

where the factor of $1/2$ is included to control for double-counting. Thus, we must prove that the objectives in Equation 14 and Equation 16 are equivalent.

First, we assume without loss of generality that the overall mean $\boldsymbol{\mu} = \sum_{i=1}^c \boldsymbol{\mu}_i = \mathbf{0}$. (Note that both Equation 14 and Equation 16 are invariant to translations in the feature space.) Then, we have

$$\begin{aligned}
\frac{1}{2} \sum_{i=1}^c \sum_{j=1}^c d_{\Sigma}(\boldsymbol{\mu}_i, \boldsymbol{\mu}_j)^2 &= \frac{1}{2} \sum_{i=1}^c \sum_{j=1}^c (\boldsymbol{\mu}_i - \boldsymbol{\mu}_j)^T \boldsymbol{\Sigma}^{-1} (\boldsymbol{\mu}_i - \boldsymbol{\mu}_j) \\
&= \frac{1}{2} \sum_{i=1}^c \sum_{j=1}^c (\boldsymbol{\mu}_i^T \boldsymbol{\Sigma}^{-1} \boldsymbol{\mu}_i + \boldsymbol{\mu}_j^T \boldsymbol{\Sigma}^{-1} \boldsymbol{\mu}_j - 2 \boldsymbol{\mu}_i^T \boldsymbol{\Sigma}^{-1} \boldsymbol{\mu}_j) \\
&= \sum_{i=1}^c \boldsymbol{\mu}_i^T \boldsymbol{\Sigma}^{-1} \boldsymbol{\mu}_i - \sum_{i=1}^c \sum_{j=1}^c \boldsymbol{\mu}_i^T \boldsymbol{\Sigma}^{-1} \boldsymbol{\mu}_j \\
&= \sum_{i=1}^c \boldsymbol{\mu}_i^T \boldsymbol{\Sigma}^{-1} \boldsymbol{\mu}_i - \left(\sum_{i=1}^c \boldsymbol{\mu}_i^T \right) \boldsymbol{\Sigma}^{-1} \left(\sum_{j=1}^c \boldsymbol{\mu}_j \right) \\
&= \sum_{i=1}^c \boldsymbol{\mu}_i^T \boldsymbol{\Sigma}^{-1} \boldsymbol{\mu}_i \\
&= \text{Tr} \left(\boldsymbol{\Sigma}^{-1} \sum_{i=1}^c \boldsymbol{\mu}_i \boldsymbol{\mu}_i^T \right) \\
&= c \text{Tr} (\boldsymbol{\Sigma}^{-1} \mathbf{S}_{\mathbf{z}})
\end{aligned}$$

In the first five lines we expanded the squared Fisher-Rao distance, used the linearity of the dot product and the fact that $\boldsymbol{\mu} = \mathbf{0}$. In the last two lines we used the linearity and the cyclic property of the trace, and that $\sum_{i=1}^c \boldsymbol{\mu}_i \boldsymbol{\mu}_i^T = c \mathbf{S}_{\mathbf{z}}$ because $\boldsymbol{\mu} = \mathbf{0}$. This shows that the objectives in Equation 14 and Equation 16 are equivalent.

C Regularization and invariance

C.1 Invariance of affine-invariant distance

To better understand SQFA, it is important to consider the invariance properties of the Fisher-Rao and the affine-invariant distances.

We first analyze the invariance for the affine-invariant distance, which is equivalent to the Fisher-Rao distance for zero-mean Gaussian distributions.

If $\mathbf{G} \in GL(m)$ where $GL(m)$ is the General Linear group, composed of non-singular m -by- m matrices, then a key property of the affine-invariant distance is that

$$d_{AI}(\boldsymbol{\Psi}_i, \boldsymbol{\Psi}_j) = d_{AI}(\mathbf{G}^T \boldsymbol{\Psi}_i \mathbf{G}, \mathbf{G}^T \boldsymbol{\Psi}_j \mathbf{G}) \quad (17)$$

(in words, the affine-invariant distance is invariant to the action by congruence of $GL(m)$).

Note that the transformed matrix $\boldsymbol{\Psi}'_i = \mathbf{G}^T \boldsymbol{\Psi}_i \mathbf{G}$ for a second-moment matrix $\boldsymbol{\Psi}_i$ corresponds to the second moment matrix of the transformed variable $\mathbf{z}' = \mathbf{G}^T \mathbf{z}$ (in absence of additive regularization noise). Furthermore, if $\mathbf{z} = \mathbf{F}^T \mathbf{x}$, then \mathbf{z}' can be obtained by applying the filters $\mathbf{F}' = \mathbf{F} \mathbf{G}$ to the data \mathbf{x} , i.e. $\mathbf{z}' = \mathbf{F}'^T \mathbf{x}$. This can be summarized in the following equation:

$$\boldsymbol{\Psi}'_i = \mathbf{F}'^T \mathbb{E} [\mathbf{z} \mathbf{z}] \mathbf{F}' = \mathbf{G}^T \mathbf{F}^T \mathbb{E} [\mathbf{z} \mathbf{z}] \mathbf{F} \mathbf{G} = \mathbf{G}^T \boldsymbol{\Psi}_i \mathbf{G} \quad (18)$$

Because the second-moment matrices $\boldsymbol{\Psi}_i$ obtained with \mathbf{F} and $\boldsymbol{\Psi}'_i$ obtained with \mathbf{F}' are related by congruence by the same matrix \mathbf{G} for all classes i , all the pairwise class distances are the same for both sets of filters. Thus, if a set of filters \mathbf{F} maximizes the affine invariant distances (i.e. the objective of smSQFA), then the set of filters $\mathbf{F}' = \mathbf{F} \mathbf{G}$ also maximizes the objective function. This means that the solution (without regularizing noise) is not unique.

The same invariance property that makes the solution non-unique is true for the Fisher-Rao distance [41, 46], and of the Calvo-Oller bound. To see this, let $\mathbf{H} = \begin{bmatrix} \mathbf{G} & \mathbf{0} \\ \mathbf{0} & 1 \end{bmatrix}$, where $\mathbf{0}$ is a m -by-1 vector of

zeros, and $\mathbf{H} \in GL(m+1)$. Then we have the following relation

$$\mathbf{H}^T \Omega_i \mathbf{H} = \mathbf{H}^T \begin{bmatrix} \Sigma_i + \mu \mu^T & \mu \\ \mu^T & 1 \end{bmatrix} \mathbf{H} = \begin{bmatrix} \mathbf{G}^T (\Sigma_i + \mu \mu^T) \mathbf{G} & \mathbf{G}^T \mu \\ \mathbf{G} \mu^T & 1 \end{bmatrix} = \begin{bmatrix} \Sigma'_i + \mu' \mu'^T & \mu' \\ \mu'^T & 1 \end{bmatrix} = \Omega'_i \quad (19)$$

where $\mu' = \mathbf{G}^T \mu$ and $\Sigma'_i = \mathbf{G}^T \Sigma_i \mathbf{G}$ are the mean and the covariance matrix of the transformed variable $\mathbf{z}' = \mathbf{G}^T \mathbf{z}$. Then, the Calvo-Oller embeddings of the class statistics Ω_i and Ω'_i obtained with the filters \mathbf{F} and $\mathbf{F}' = \mathbf{F} \mathbf{G}$ respectively, are related by congruence by the same matrix \mathbf{H} . Because of the invariance of the affine-invariant distance, if \mathbf{F} is a solution maximizing the sum of pairwise affine-invariant distances between the embeddings, then \mathbf{F}' is also a solution.

In sum, in absence of regularizing noise, there is an equivalent set of solutions, given by the sets of filters that span the same subspace. This can be a useful property, for example because there is no need to worry about scalings in the data space. But the lack of a unique solution also makes for less interpretable features (the interpretable object is the subspace spanned by the filters).

C.2 Regularization breaks invariance

The equivalence of solutions above, however, is eliminated when we introduce regularization as an additive term $\mathbf{I} \sigma^2$ to each second-moment matrix. Specifically, if we regularize the second-moment matrices by adding $\mathbf{I} \sigma^2$ to each matrix, such that $\Psi_i = \mathbf{F}^T \mathbb{E}[\mathbf{z} \mathbf{z}] \mathbf{F} + \mathbf{I} \sigma^2$, then it is no longer true that $\Psi'_i = \mathbf{G}^T \Psi_i \mathbf{G}$. Rather, there will be a different matrix \mathbf{G}_i satisfying $\Psi'_i = \mathbf{G}_i^T \Psi_i \mathbf{G}_i$ for each class i . Thus, Equation 17 no longer relates the distances for filters \mathbf{F} and $\mathbf{F}' = \mathbf{F} \mathbf{G}$, and the distances between second-moment matrices are no longer the same for both sets of filters.

One consequence of adding regularization is that the solution is no longer scale invariant. For filters with small norms, matrices $\Psi_i = \mathbf{F}^T \Phi_i \mathbf{F} + \mathbf{I} \sigma^2$ will be dominated by the regularization term, and thus more similar (i.e. closer) to each other. Then, the solution will tend towards filters with infinite norm that make the contribution of the regularization term negligible. In our case the filters (i.e. each column of \mathbf{F}) are constrained to have unit norm, so this is not a problem.

Following the same reasoning, the regularization term will penalize filters that lead to small second-moment matrices, since these will be dominated by the regularization term. Thus, regularization will favor the directions in the data space that lead to larger second-moment matrices. This might be useful in that it makes the filters more robust to estimation noise along dimensions with small variance, but it might also mask important information in directions with low squared values. Also, this makes the results dependent on the choice of the regularization parameter σ^2 . Future work should explore the effect of regularization on the features learned by SQFA, and examine how to choose the regularization parameter.

We note that regularization does not break the invariance of filter polarity, that is, the sign of the filters, and thus different runs of SQFA might lead to different signs of the filters.

D Training times

For each dataset, we recorded the time it took to train the models on a consumer laptop with an 12th Gen Intel Core i7-1270P and 32 GB of RAM.

SQFA training times were in the order of seconds for all datasets (Figure 12). Remarkably, the training time for SQFA was comparable to that of LDA, ICA and FA, which are computationally efficient linear methods. It is worth noting that, while computing the affine-invariant distances involves computing the matrix inverse square root, which can be computationally expensive, this operation is only done for the second-moment matrices in the feature space in the case of smSQFA, and the embeddings in Equation 4 for SQFA. These are small matrices of size $m \times m$ for smSQFA and $m+1 \times m+1$ for SQFA. Thus, in cases where m is not large, the cost of each SQFA iteration is not high.

We note that SQFA training times were higher for the speed estimation dataset compared to the other datasets. This is partly because the filters were learned sequentially for this task, which is more computationally expensive than learning all filters at once.

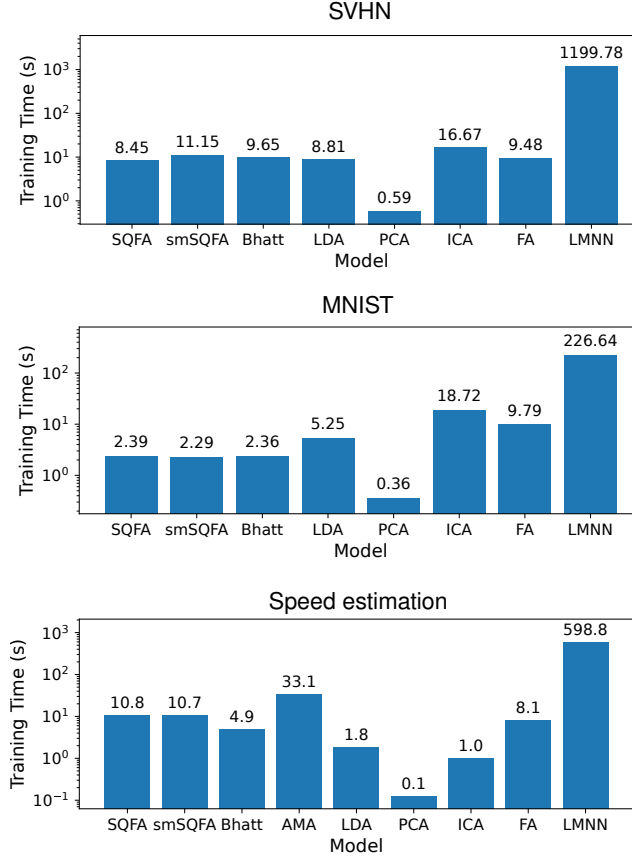


Figure 12: Training times for the different models on the different datasets. Times are in seconds, and indicated by the numbers on top of each bar. The y-axis is logarithmic. **Left:** SVHN. **Center:** MNIST. **Right:** Speed estimation dataset. We note that LMNN was trained on reduced datasets compared to the other methods (see Section 2.5).

E Gaussian testing datasets

To better understand the performance of SQFA relative to other methods, it is useful to know to what extent the non-Gaussianity of the data affects the performance of the different methods. For example, the Fisher-Rao and Bhattacharyya distances used here both assume that the data is Gaussian. Are the relative performances of the two methods due to how well they capture Gaussian discriminability, or because of how robust they are to non-Gaussianity? To answer this question, we tested the learned filters on a synthesized testing dataset, where for each class we generate a set samples (20000 for the digit recognition datasets, 5000 for the speed estimation dataset) from a Gaussian distribution with the same mean and covariance as the training data for that class. We also added independent Gaussian noise to each sample matching the regularization noise used in training.

We see in Figure 13 that the relative performance of the different methods is similar to that observed in the original datasets.

F Details of the motion estimation task

F.1 Dataset synthesis

The motion estimation dataset consists of synthetic naturalistic videos of surfaces moving at different frontoparallel speeds, that were synthesized following the procedure described in [7].

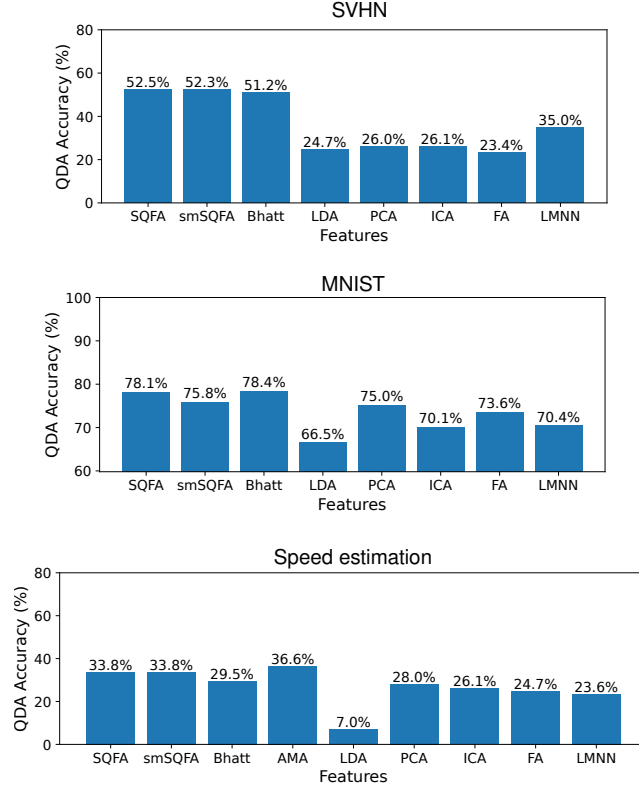


Figure 13: QDA accuracy for each of the datasets, using testing data generated from Gaussian distributions matching the mean and covariance of the training data. From top to bottom, the datasets are SVHN, MNIST, and the speed estimation dataset.

Briefly, each video is initially 60-by-60 pixels and 15 frames long. In this synthesis procedure, 60 pixels correspond to 1 degree of visual field (roughly equivalent to the foveal sampling of photoreceptors) and the videos have a duration of 250 ms (roughly equivalent to the duration of a fixation in natural viewing).

A video is synthesized by taking a random patch from an image of a natural scene and moving it horizontally at a given speed behind a 60-by-60 pixel aperture, for a duration of 15 frames. The resulting video is then filtered spatiotemporally to simulate the response of retinal photoreceptors to the video, following the procedure described in [26]. Then, the resulting video is downsampled spatially by a factor of 2, to 30-by-30 pixel frames, and each frame is averaged vertically, leading to 30 pixel by 15 frame videos (thus, each video can be represented as a 450 dimensional vector). Vertically averaging the movies is equivalent to only considering filters that are vertically-oriented in the original 2D frame videos.

Then, to simulate further retinal processing, the video is converted to contrast, by subtracting and dividing by its mean intensity across pixels and frames. Denoting the resulting contrast video by \mathbf{c} , we apply divisive normalization to the video, dividing it by $\sqrt{(\|\mathbf{c}\|^2 + nc_{50}^2)}$ where $c_{50}^2 = 0.045$ is a constant and $n = 450$ is the number of pixels in the video multiplied by the number of frames. The resulting video simulates the retinal output in response to a naturalistic motion. Further discussion of this synthesis procedure can be found in [7, 26].

Above, we described the process by which a video is synthesized for a given speed. In the dataset, 41 retinal speeds (i.e. classes) were used, ranging from -6.0 to 6.0 deg/s with 0.3 deg/s intervals. For each of the 41 retinal speeds, we synthesized 800 different naturalistic videos, by using a different randomly sampled patch from a natural scene for each video. This adds nuisance naturalistic variability to the dataset. We used 500 videos per speed for training (a total of 20500 videos) and 300 videos per speed for testing (a total of 12300 videos).

Note that because the videos are generated with small patches randomly sampled from natural images, the expected intensity value at each pixel and frame is approximately the same (because natural image patches are approximately stationary), independent of speed. Then, because the videos were constrained to be contrast videos—i.e. they are formed by subtracting off and dividing by the intensity mean, consistent with early operations in the human visual system[7]—the mean across patches equals zero, independent of speed. This results in a dataset where the classes are all approximately zero-mean.

F.2 AMA-Gauss training

The AMA-Gauss model was implemented as described in [28, 26]. First, a set of linear filters \mathbf{F} is applied to each pre-processed video, and a sample of independent noise is added to each filter output. This results in a noisy response vector $\mathbf{R} = \mathbf{F}^T \mathbf{c} + \lambda$, where $\lambda \sim \mathcal{N}(0, \mathbf{I}\sigma^2)$ is the added noise. Then, a QDA-like decoder is used to classify the videos based on the noisy response vectors, assuming that the noisy response vectors are Gaussian distributed conditional on the speed (i.e. the class). The decoder computes the likelihood of the response given each class, that is, $p(\mathbf{R}|y = i)$, and using the priors (which we set as flat) and Bayes rule, it computes the posterior distribution $p(y|\mathbf{R})$ for the different speeds. For a given video \mathbf{c} corresponding to true class $y = j$, the AMA-Gauss training loss is the negative log-posterior at the correct class, that is, $-\log p(y = j|\mathbf{R})$. The filters \mathbf{F} that minimize the loss are obtained using gradient descent. The filters (columns of \mathbf{F}) are constrained to have unit norm. We use the same regularization parameter σ^2 for AMA-Gauss and for SQFA. AMA-Gauss filters were learned in a pairwise fashion.